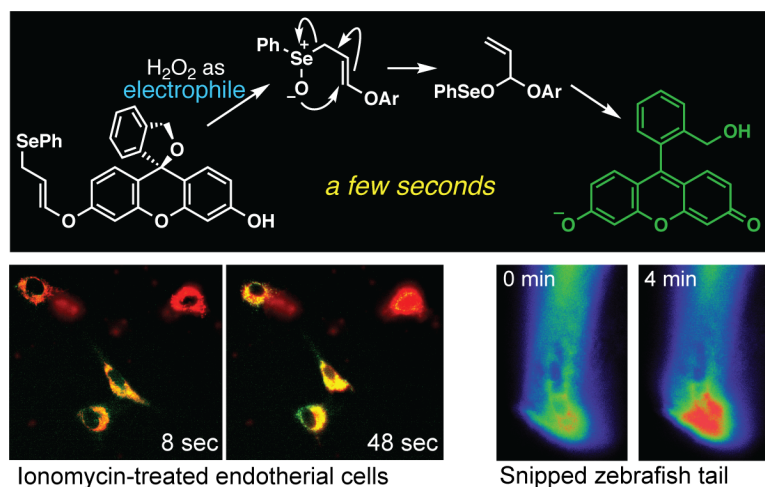


Fluorogenic Probe Using a Mislow-Evans Rearrangement for Time-Resolved Imaging of Hydrogen Peroxide

Dianne Pham¹, Upamanyu Basu¹, Ivanna Pohorilets¹, Claudette M. St Croix², Simon C. Watkins², and Kazunori Koide^{1*}

¹Department of Chemistry, University of Pittsburgh, 219 Parkman Avenue, Pittsburgh, Pennsylvania 15260, United States

²Center for Biologic Imaging, Department of Cell Biology, University of Pittsburgh, 3500 Terrace Street, Pittsburgh, Pennsylvania 15261, United States



Abstract: Hydrogen peroxide (H_2O_2) is a second messenger that mediates the biology of wound healing, apoptosis, inflammation, aging, neurodegenerative diseases, and more. Its presence has been fluorometrically imaged with protein- or small molecule-based sensors. However, only protein-based sensors have afforded temporal insights with the resolution of seconds. Small molecule-based fluorogenic probes are preferred for various reasons; however, current electrophilic chemosensors react with H_2O_2 slowly, requiring >20 minutes for a sufficient response. Here, we report a fluorogenic probe that selectively reacts with H_2O_2 and undergoes a [2,3]-sigmatropic rearrangement (seleno-Mislow-Evans rearrangement) followed by an acetal hydrolysis to produce a green fluorescent molecule in seconds. The mode of reaction is based on the umpolung of previously developed sensors; the probe acts as a nucleophile rather than an electrophile. The fast kinetics outcompete the reaction between thiols and H_2O_2 , enabling real-time imaging of H_2O_2 produced inside the subcellular compartments of cells in 8 seconds. Further, the probe was able to recapitulate data previously observed only with a genetically encoded protein-based sensor. The present probe design provides a platform that can match the temporal resolution of protein-based H_2O_2 detection.

Introduction

Hydrogen peroxide (H_2O_2) is a reactive oxygen species (ROS) involved in many biological processes. As such, misregulation of H_2O_2 has been implicated in many diseases.¹⁻² In the cell, H_2O_2 is produced along with other ROS in the mitochondria and cytoplasm by the NADPH oxidase (NOX) family of enzymes, xanthine oxidase,

and cytochrome P450 enzymes.^{1,3} In light of the dichotomous nature of H₂O₂ in maintaining cellular homeostasis, it has become increasingly important to understand the detailed biology of H₂O₂.

Only recently has the spatiotemporal presence of H₂O₂ in wound healing been recognized.⁴⁻¹⁰ Additionally, ROS production is critical for defense against pathogens; however, early studies used nonselective probes for ROS and could not distinguish between effects caused specifically by H₂O₂.¹¹⁻¹⁴ Studies of biological H₂O₂ with high specificity and temporal resolution have relied on genetically encoded protein sensors.¹⁵⁻¹⁶ These studies using protein-based sensors have revealed that upon injury to tissue, H₂O₂ is produced to recruit immune cells to counteract infection; in wound healing, H₂O₂ gradients are formed in seconds to minutes from the site of injury, facilitating the mobilization of immune cells.¹⁵ These results have not been observed using chemical probes, likely due to the comparatively slow reaction kinetics.

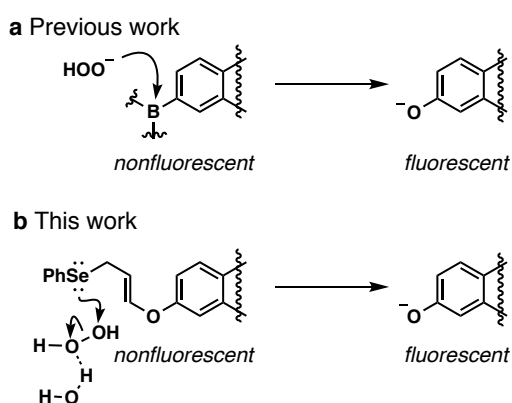


Figure 1. Comparison of (a) boronate-based and (b) selenium-based probes for hydrogen peroxide.

Most sensors for H₂O₂ have relied on the boronate ester functionality (Figure 1a) for reaction,¹⁷ although other functionalities have been reported.¹⁸⁻²¹ Advances from these studies have allowed for selective detection of H₂O₂ over other reactive oxygen and nitrogen species (RNS). This chemistry presumably requires the presence of the hydroperoxide anion, HOO⁻. Under biological conditions, the abundance of this species should be very low (~0.1% of H₂O₂) because the pK_a of H₂O₂ is 11.6.

To develop a new probe to more rapidly react intracellularly, in this study we used the seleno variant of the Mislow-Evans rearrangement, which requires the oxidation of the allylic selenide by H₂O₂.²²⁻²³ This rearrangement is fast even at 0 °C²⁴ and requires the neutral and abundant form of H₂O₂ to act as an electrophile (Figure 1b); this reactivity has not been exploited in the development of chemosensors for this ROS. We hypothesized that the seleno Mislow-Evans rearrangement would provide a novel platform for the fluorometric detection of H₂O₂ with superior kinetics to more favorably compete with the degradation of H₂O₂ in cells. Here, we integrate the rearrangement with a spontaneous hydrolysis of the resulting acetal to translate the high reactivity

of a selenium atom with H_2O_2 into the requisite fluorogenic switch. We present the synthesis of the allylic selenide **1** and its selectivity for H_2O_2 over other ROS and RNS. We also show that selenide **1** can detect endogenously produced H_2O_2 by treatment with ionomycin in RAW macrophages and in a zebrafish tail wound-healing experiment.

Results

Probe design. We envisioned that allylic selenide **1** (Figure 2a) could undergo oxidation with H_2O_2 through transition state **TS1**, followed by the Mislow-Evans rearrangement of selenoxide **2** and the subsequent hydrolysis of selenenate **3** to form the brightly fluorescent phenoxide **5**. For the conversion of **3** to **5**, two pathways are plausible. The first pathway is the nucleophilic cleavage of the Se-O bond of **3** to form hemiacetal **4**, which spontaneously forms phenoxide **5** and acrolein (Pathway 1). The second is the oxidation of selenenate **3** to seleninate **6** en route to phenoxide **5** via hemiacetal **4** (Pathway 2). As shown below, we experimentally determined the actual pathway.

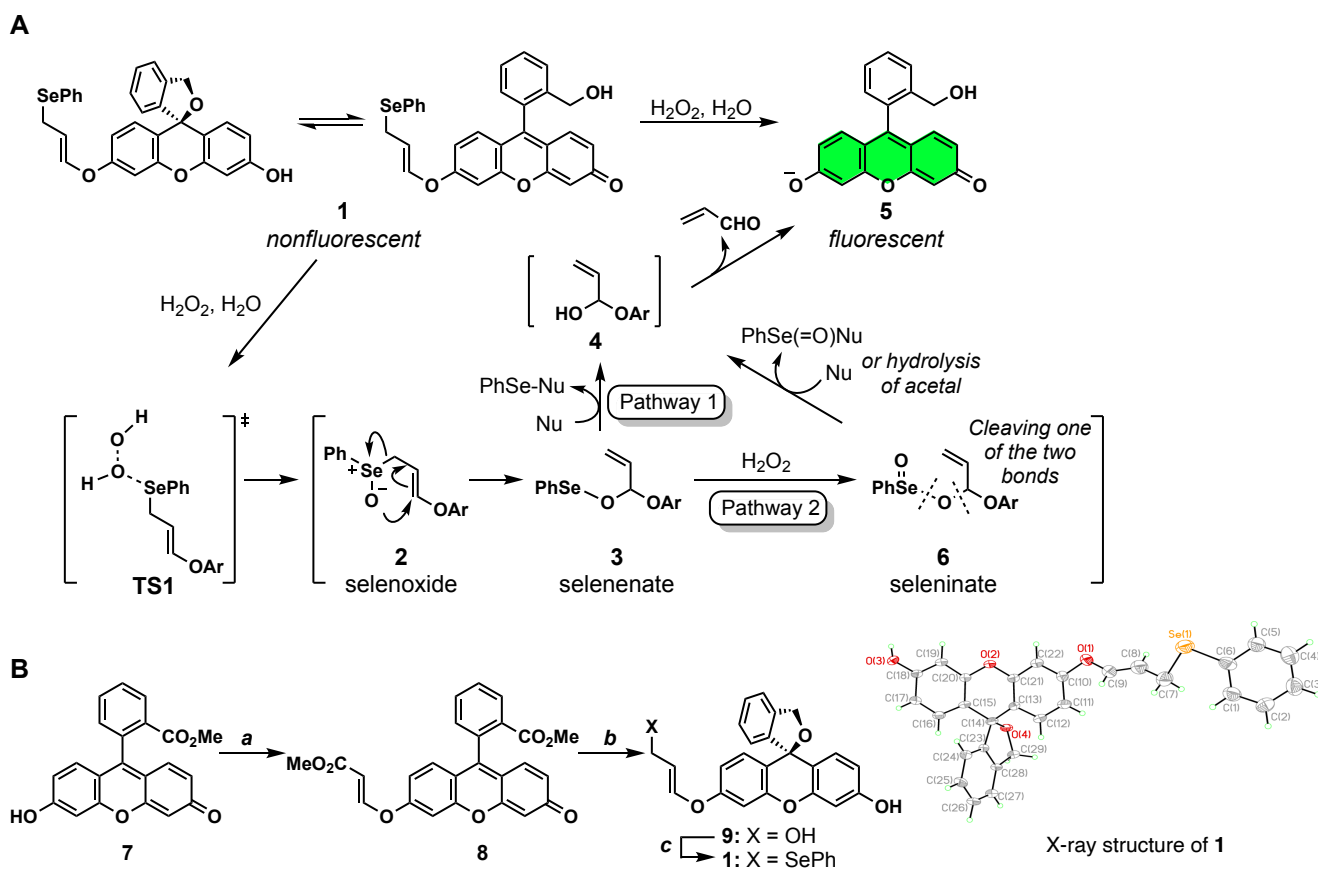


Figure 2. (A) Design of H_2O_2 probe **1** based on the seleno-Mislow-Evans rearrangement followed by hydrolysis via two possible pathways. (B) Synthesis of probe **1**. Conditions: (a) *N*-Methylmorpholine (0.3 equiv), methyl

propiolate (5.0 equiv), CH₂Cl₂, 24 h, 79 %; (b) DIBALH (7.8 equiv), CH₂Cl₂, -78 to 23 °C, 2 h; then DDQ (1.1 equiv), Et₂O, 3 h, 0 °C, 66 %; (c) ⁿBu₃P (1.2 equiv), PhSeCN (1.0 equiv), THF, 0 °C, 30 min, 41 %.

Synthesis. The synthesis of selenide **1** (Figure 2b) commenced with the conjugate addition of fluorescein methyl ester **7** to methyl propiolate to afford ester **8** in 79% yield. The following DIBALH reduction formed alcohol **9** in 66% yield. The moderate yield was caused by the hydrolysis of the enol ether during aqueous workup. The final Mitsunobu-type reaction²⁵ afforded selenide **1** in 41% yield. The structure was confirmed by the X-ray structure analysis. Similarly, the dichloro analogue **S4** was synthesized starting from **S1** (see the Supporting Information for detail), which was not used in this study due to lower yields and stability during storage.

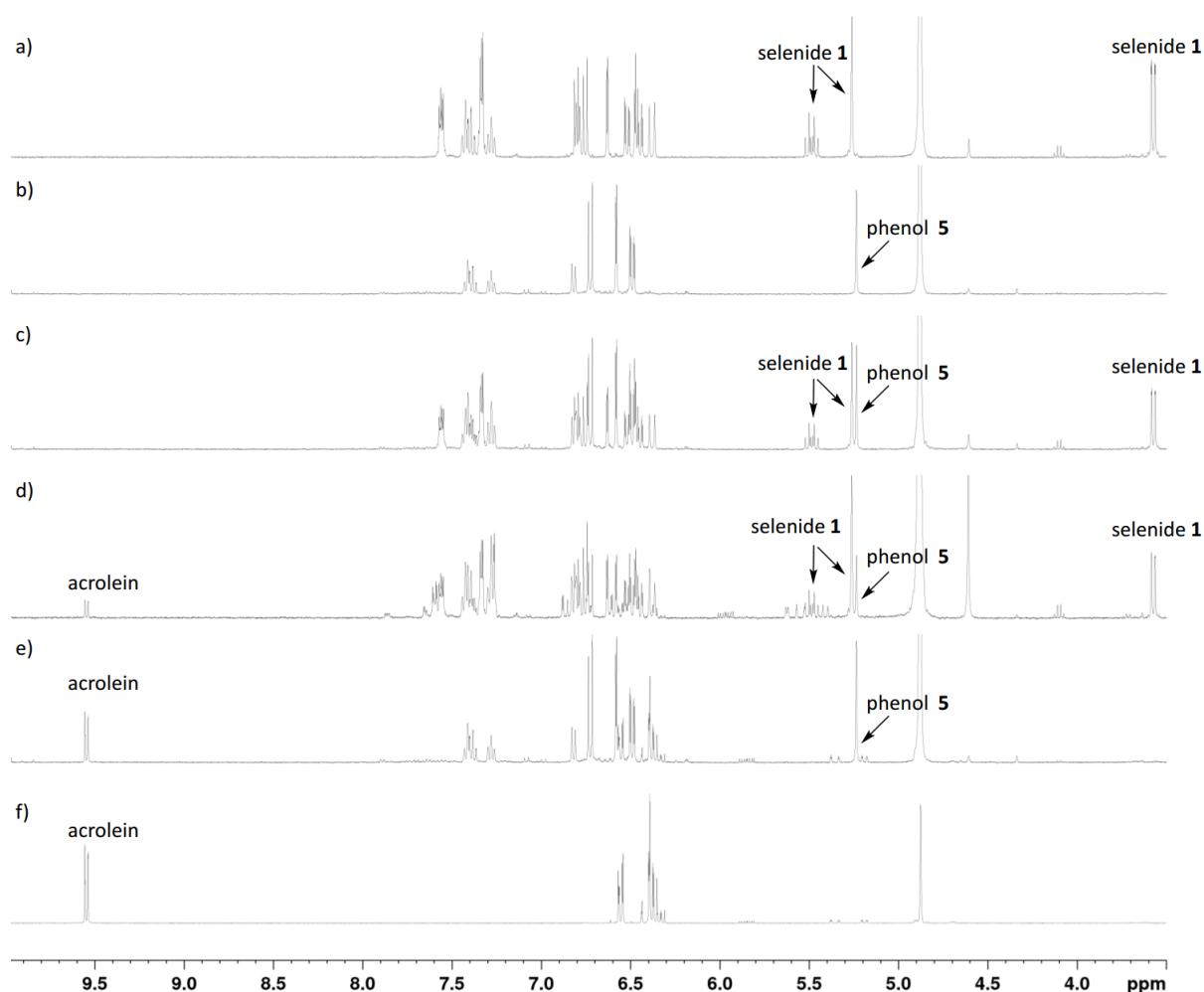


Figure 3. Mechanistic studies ¹H NMR (400 MHz, CD₃OD) spectra of (a) selenide **1**, (b) phenol **5**, (c) selenide **1** and phenol **5** (1:1), (d) crude reaction mixture of selenide **1** and H₂O₂, (e) acrolein and phenol **5** (1:1), (f) acrolein.

Mechanistic studies. To investigate the mechanism of the reaction between selenide **1** and H₂O₂ as depicted in Figure 2a, we monitored the reaction in situ by ¹H NMR spectroscopy. Figure 3a, Figure 3b, and Figure 3c show selenide **1**, phenol **5**, and a 1:1 mixture of **1** and **5**, respectively, in CD₃OD. Upon treatment of the selenide with substoichiometric amounts of H₂O₂, both phenoxide **5** and acrolein were formed (Figure 3d; for an authentic mixture of phenol **5** and acrolein and for acrolein alone, see Figure 3e and Figure 3f), supporting our proposed design for the H₂O₂ detection strategy. The HPLC chromatograms (Figure S1, Supporting Information) revealed that the reaction of selenide **1** with H₂O₂ produced phenol **5**, but did not produce PhSeO₂H. Therefore, pathway 1 (Figure 2a) is operative under these conditions leading to the formation of the putative intermediate PhSeOH as a side product.

Stability of 1. Since organic selenides are known to be prone to oxidative decomposition in air,²⁶ we investigated the stability of **1** under ambient conditions. The ¹H NMR analysis of **1** in DMSO-*d*₆ showed that **1** underwent cis-trans isomerization of the enol ether with a half-life of 60 days (Figures S2 and S3, Supporting Information). Even so, the compound was quite resistant to oxidative decomposition up to 60 days as manifested by the presence of only less than 10% acrolein. The cis-trans isomerization and further decomposition were more pronounced in protic solvents such as CD₃OD or in CDCl₃ that may contain trace DCl.

As evident from Figure S4 and Table S1 (Supporting Information), the difference in fluorescence intensity of **1** the product, phenol **5**, is 27-fold. Generally, *O*-alkylation of Pittsburgh Green suppresses the fluorescence by 200–400 fold.²⁷ The somewhat modest increase in the current work (27-fold) in fluorescent turn-on signal is attributed to the trace contamination of the fluorescent compound **5** during the purification of the non-fluorescent probe **1**. From the standard calibration curve (Figure S4), the estimated amount of **5** in **1** as an impurity was calculated to be 2.5%, leading to a 5–10 times higher background signal. Thus, if trace phenoxide **5** can be removed from selenide **1** (HPLC did not improve the purity of **1**), the signal increase in the conversion of **5** to **1** should be 125–250 fold. Nevertheless, the trace amount of **5** in **1** does not affect the calculation of rate constant shown below (Figure 4).

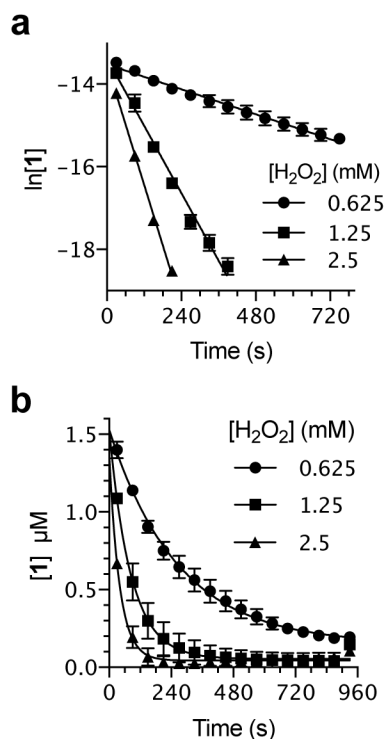


Figure 4. (a) plot of $\ln[1]$ vs t to obtain slope (k') and (b) plot of $[1]$ vs time. For (a), $Y = -0.002514X - 13.52$ ($R^2 = 0.8939$) for 0.625 mM H_2O_2 , $Y = -0.01359X - 13.38$ ($R^2 = 0.9792$) for 1.25 mM H_2O_2 , and $Y = -0.02432X - 13.51$ ($R^2 = 0.9978$) for 2.5 mM H_2O_2 .

Kinetics. With the fluorometrically measured concentrations of selenide **1** shown in Table S3 (Supporting Information), $\ln[1]$ versus time (s) was plotted to obtain observed rate constants k' as the slope of the linear plot (Figure 4a). To determine the second-order rate constant of the reaction of **1** with H_2O_2 , a solution of **1** in 5% MeCN in a pH 7.5 HEPES buffer was diluted with H_2O_2 in a 96-well plate, and the progressive increase in fluorescence was recorded using a plate reader. The relative fluorescence was measured every minute until the reaction was completed. The fluorescence readout was converted to the amount of phenol **5** formed using a standard curve for the phenol concentration versus fluorescence intensity (Figure S5). Based on the pseudo first-order kinetic studies (Figure 4b), the second-order rate constant k of the reaction was calculated (details in Supplementary Material, Figure S6 and Table S3) to be $9.82 \pm 1.11 M^{-1}s^{-1}$. Similarly, the pseudo-first order kinetics of the reaction between **S4** and H_2O_2 was studied (Figures S7–S9 and Tables S5 and S6, Supporting Information); the second-order rate constant was $9.33 \pm 0.64 M^{-1} s^{-1}$.

Selenide 1 reacts with H_2O_2 in a concentration dependent manner. To verify that **1** could quantitatively measure H_2O_2 concentrations, we incubated **1** with increasing concentrations of H_2O_2 . Fluorescence increased linearly with H_2O_2 concentration (Figure 5a), indicating that the probe could be used to quantify H_2O_2 .

Selectivity of **1 towards H_2O_2 .** Following the kinetic studies, the selectivity of **1** was assessed against other ROS and RNS; these included $O_2^{\cdot-}$, 1O_2 , $\cdot OH$, ClO^- , $ONOO^-$, $tBuOOH$, NO_3^- , NO_2^- , and $NO\cdot$. Relative to H_2O_2 , little

reaction was observed with other ROS (Figure 5b). We controlled for the fact that the production of some of these ROS required H₂O₂ as a reagent (see Supplementary Information for details). Thus, we concluded that **1** was selective for H₂O₂ over other ROS and RNS.

To determine whether the probe reacts with O₂^{•-}, KO₂ was added to a solution of **1** buffered at pH 7 for 15 min and compared to the reaction with H₂O₂. Since O₂^{•-} is known to spontaneously dismutate to form H₂O₂, increasing amounts of catalase were added to the samples containing KO₂ to ensure that **1** did not react with any of the in-situ-generated H₂O₂. Selenide **1** reacted readily with H₂O₂, while the observed fluorescence from the samples containing KO₂ decreased with increasing catalase concentrations (Figure S12), indicating that **1** did not react with O₂^{•-}. Therefore, **1** is selective for H₂O₂ over O₂^{•-}.

We employed various controls when testing the selectivity of selenide **1** with ¹O₂, formed by the reaction of Na₂MoO₄ with H₂O₂.²⁸ A large fluorescence increase was observed only in the samples containing 100 μM of both Na₂MoO₄ and H₂O₂ (Figure S12). No fluorescence increase was observed in samples containing only Na₂MoO₄, indicating that the probe was not reacting with the Na₂MoO₄. Together, these results suggested that the probe may have reacted with ¹O₂. However, the addition of NaN₃, a known ¹O₂ scavenger,²⁹⁻³⁰ did not decrease the fluorescence. Thus, we concluded that the fluorescence observed was not caused by the reaction of **1** with ¹O₂, but rather the H₂O₂ required to produce it. 10⁴ U/mL catalase was added to the solutions to verify that **1** indeed responded to excess H₂O₂ that had not reacted with the Na₂MoO₄. The addition of catalase abolished the fluorescence signal observed in the presence of high concentrations of H₂O₂ (Figure S12).

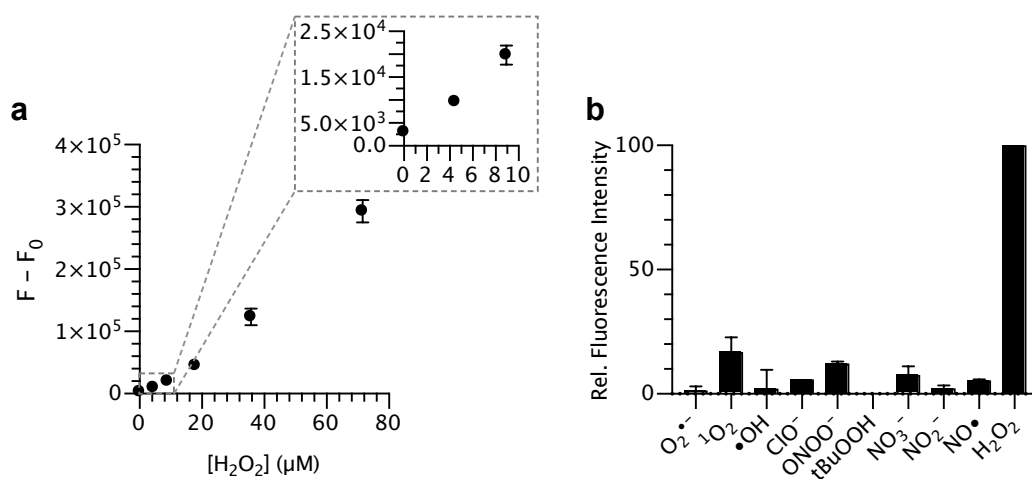


Figure 5. The fluorescence response of **1** (1 μM) at pH 7 (a) with increasing concentrations of H₂O₂ or (b) various ROS. (a) 10 μM **1**, 0–71.5 μM H₂O₂, 14.5:85.5 MeCN/50 mM phosphate pH 7, (b) Data were normalized so that the reaction of **1** and H₂O₂ was set to 100. Excess ROS and RNS compared to **1** was used.

The reactivity of **1** with •OH was also investigated. •OH was generated from the reaction of Fe²⁺ with H₂O₂.³¹ A solution of **1** was titrated with FeSO₄ and H₂O₂. Fluorescence did not increase as the concentration of

FeSO₄ increased (Figure S13), indicating that neither FeSO₄ nor the •OH reacted with the probe. Addition of catalase to the solution reduced fluorescence intensity, indicating that the enhanced signals were caused by the reaction of the probe with the H₂O₂ required to produce •OH.

Next, we tested whether OCl⁻, ONOO⁻, and ^tBuOOH would react with **1**. No statistically significant increase in fluorescence intensity was observed with increasing concentrations of OCl⁻ (Figures S14 and S15). A slight increase in fluorescence intensity was observed with increasing ONOO⁻ concentration (Figure S14). We assessed the reactivity against ^tBuOOH; no fluorescence was observed even at 10 μM ^tBuOOH (Figure S15). The minute or negligible fluorescence signals observed in these studies led us to conclude that the tested ROS do not interfere with the **1**-based fluorometric method for H₂O₂.

We then sought to determine whether RNS would react with **1** to produce fluorescence. **1** was exposed to either NO₂⁻, NO₃⁻, or NO• at various concentrations. The fluorescence change over the first 15 min was reported for NO₂⁻ and NO₃⁻ in Figure S16 and S17, respectively. No concentration dependence was observed with either NO₂⁻ or NO₃⁻ indicating that **1** did not react with these RNS. Similar results were obtained for NO• (Figure S18). These data suggest that **1** did not react with NO₂⁻, NO₃⁻, nor NO•.

Cellular Imaging with 1. We then attempted to image H₂O₂ within cells. HeLa cells were incubated with 0.5 μM **1** for 15 min prior to imaging. After washing with HBSS and replacing the media, H₂O₂ was added. Within 30 s, a significant increase in fluorescence was observed in HeLa cells (Figure 6a). Punctate fluorescence was observed in cytoplasm, suggesting that **1** may localize within mitochondria. We then attempted to monitor endogenous ROS production upon stimulation with ionomycin (final concentration: 10 μM) in RAW cells, which is more biologically relevant than the exogenous addition of H₂O₂.³² A significant response was observed within 30 s of addition of ionomycin relative to the baseline fluorescence (Figure 6b and Figure 6c) and peaked at 48 s.

To confirm the mitochondrial localization of **1**, endothelial cells were simultaneously treated with **1** and MitoTracker Red for 20 min (Figure 6d). The first image taken 8 s after the addition of ionomycin (final concentration: 10 μM) already showed increased fluorescence, and time-lapse imaging showed that fluorescence continued to increase over time. The overlap of the green and red fluorescence indicated that the probe was indeed localizing to mitochondria. However, the Pearson correlation coefficient was 0.114 ± 0.034 , suggesting that although some overlap with mitochondria was observed, the bulk of the green fluorescence was observed outside of mitochondria. Furthermore, the diffusion of both the green and red fluorescence indicated that stimulation with ionomycin likely induced changes in mitochondrial membrane potential or permeability causing the contents to leak out.

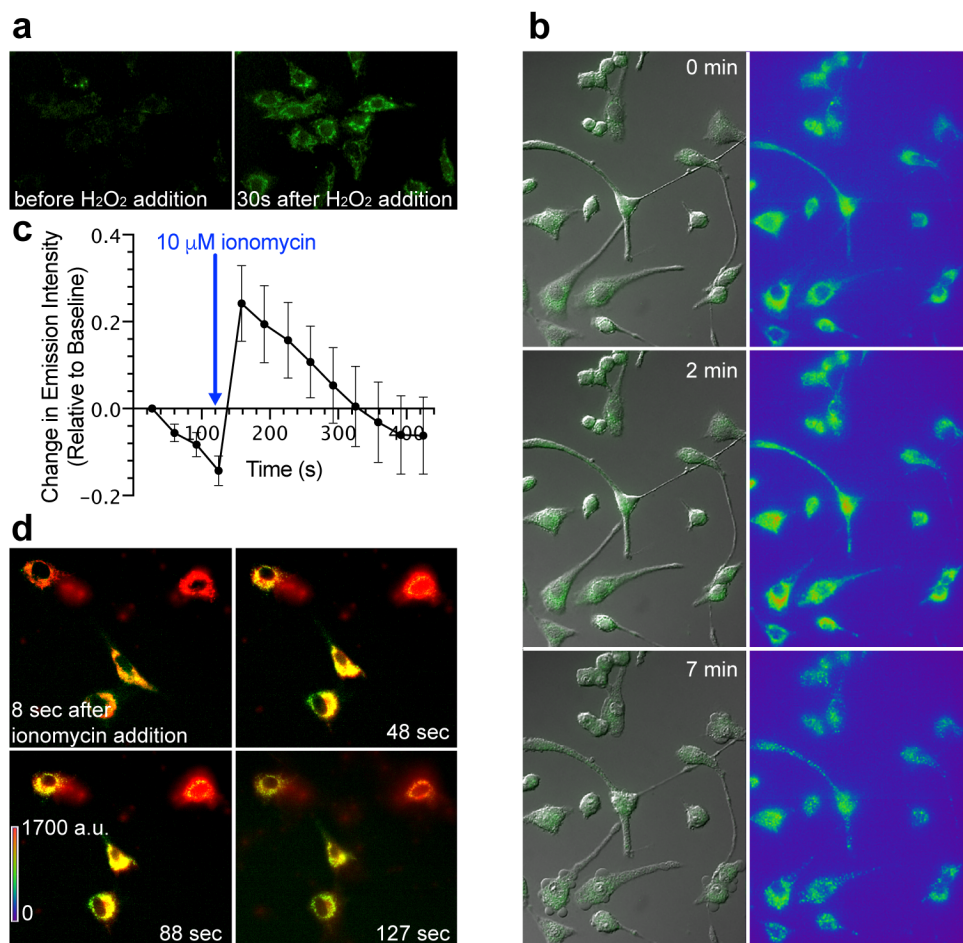


Figure 6. Cellular images using **1**. (a) HeLa cells treated with **1** showed a significant fluorescence increase after the addition of H₂O₂. Cells were loaded with **1** for 15 min and washed prior to imaging. H₂O₂ was added while imaging. (b) RAW macrophages loaded with 0.5 μM **1** showed (c) a significant response within 30 s of addition of ionomycin (final concentration: 10 μM). Fluorescence channel (green) and pseudo-color shown. (d) Endothelial cells loaded with **1** and MitoTracker Red were stimulated with ionomycin. Colocalization studies revealed increased green fluorescence intensity found localized to mitochondria, suggesting mitochondrial production of H₂O₂.

***In vivo* imaging with **1**.** To date, only protein-based fluorescent sensors have been able to illuminate the spatiotemporal dynamics of H₂O₂ *in vivo*. We hypothesized that our method might be rapid enough to match the protein-based imaging *in vivo*. As a platform to test this hypothesis, we applied **1** to image a zebrafish tail wound-healing model. Fish were loaded with 1 mM **1** for 2 h before anesthetizing and mounting them in agarose. The tail fin was subsequently snipped, and the images were taken every 60 s. We observed an increase in fluorescence intensity, with the fluorescence at a maximum approximately 10–20 min after tail snipping. As shown in Figure 7, the probe was capable of providing the spatiotemporal information that matches the previous report.¹⁵

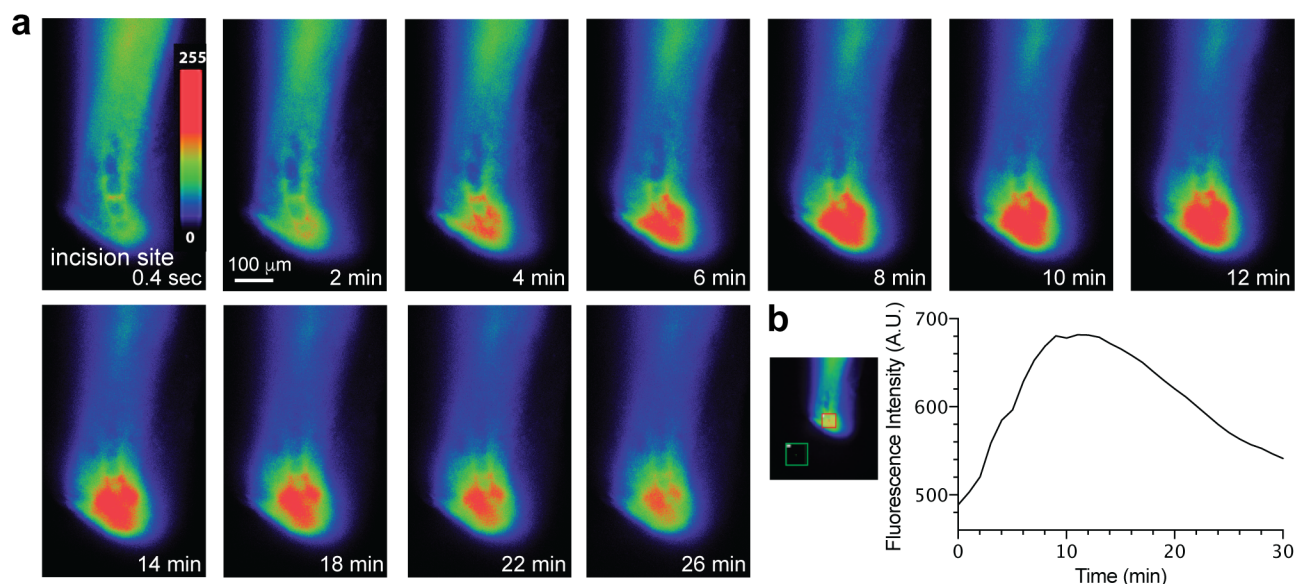


Figure 7. Imaging of H₂O₂ in zebrafish wound-healing model. (a) Snap shots of the fluorescence imaging of wound-induced H₂O₂. Zebrafish were loaded with **1**, then had the tails snipped. H₂O₂ was produced at the incision site over the course of 30 min. The original movies are available in the Supplementary Information. (b) The fluorescence intensity over time. The Y-axis = fluorescence intensity in the red square – fluorescence intensity in the green square.

Discussion

As shown in Figure 2a, the reaction of selenide **1** with H₂O₂ forms selenoxide **2**. This intermediate immediately undergoes a very rapid [2,3]-sigmatropic rearrangement to generate selenenate **3**. The oxidation of selenium is expected to be faster than that of biological sulfur compounds as H₂O₂ reacts faster with selenium than with sulfur. Hence, cellular thiols should not severely interfere with the present method.³³ From the selenenate, we envisioned two pathways leading to phenoxide **5**. In pathway 1, a nucleophile, such as a thiol or water, attacks the selenium atom to cleave the Se-O bond to form phenoxide **5** through the hemiacetal intermediate **4**. In pathway 2, selenenate **3** is further oxidized to seleninate **6**. The subsequent hydrolysis of the acetal or a nucleophilic attack toward the selenium yields phenoxide **5** through **4**. To our knowledge, these two pathways have not been experimentally investigated. Based on the aforementioned results, we propose that pathway 1 is more likely since PhSe(=O)OH, when water was the only plausible nucleophile, was not detected.

Our kinetic studies indicated that **1** reacted with H₂O₂ seven times faster than boronate-based probes. The superior kinetics will be useful for spatiotemporal imaging of biological H₂O₂; furthermore, the second-order rate constant for the reaction of **1** with H₂O₂ was of the same order of magnitude as the reaction of thiols with H₂O₂.

Studies assessing the selectivity among ROS and RNS require careful planning because several ROS either degrade to form H₂O₂ or require the input of H₂O₂ to produce the ROS. Our careful control ensured that we were monitoring the desired ROS. We observed only minor fluorescence increases in the presence of other ROS

and RNS besides H₂O₂. To verify that **1** does not react with O₂^{•-}, we added catalase to react with H₂O₂ generated from the dismutation of O₂^{•-}. Fluorescence decreased with increasing concentrations of catalase (Figure S11), indicating that **1** had been reacting with H₂O₂ and not with O₂^{•-}. Similar controls were employed to assess the selectivity of **1** against ¹O₂ and •OH. ¹O₂ or •OH was formed upon the addition of H₂O₂ to Na₂MoO₄ or FeSO₄, respectively. With high concentrations of both H₂O₂ and NaMoO₄, a solution of **1** fluoresced strongly (Figure S12). However, when NaN₃ was added under the same conditions to quench ¹O₂, the fluorescence signal remained the same as the result with H₂O₂ without Na₂MoO₄, indicating that **1** reacted with H₂O₂ and not with ¹O₂. This was confirmed when catalase prevented **1** from producing the fluorescence signal (Figure S12). Figure S13 shows that selenide **1** does not react with •OH, as the fluorescence signal intensities were not correlated with FeSO₄ concentrations, and the fluorescence increase was only due to the presence of unreacted H₂O₂. It is unlikely that the addition of catalase consumed the entirety of the H₂O₂ added because the reaction of H₂O₂ with the metals occurs rapidly to form ROS.³⁴

We also observed negligible reactivity towards ClO⁻, ONOO⁻, and ^tBuOOH (Figures S14 and S15). A cautionary note is that high concentrations of ONOO⁻ reacted with selenide **1**, but this may be attributed to trace amounts of H₂O₂ in the ONOO⁻ solution.³⁵ Furthermore, it is highly unlikely that ONOO⁻ would react with **1** under aqueous conditions because, once protonated, has only a half-life of 1.9 s at pH 7.4.³⁶ Similarly, no fluorescence was observed upon the addition of NO₂⁻, NO₃⁻, nor NO• (Figure S16–18). Altogether, our results indicate that selenide **1** is a highly selective chemosensor for H₂O₂.

Our imaging experiments indicated that selenide **1** could be applied to assess biological questions. Selenide **1** instantaneously responded to both exogenously applied and endogenously produced H₂O₂, indicating its applicability in gaining new spatiotemporal insights into cellular pathways involving H₂O₂. The fluorescence was the strongest in the mitochondria, the cellular compartments that produce H₂O₂. To our knowledge, this is the first time that H₂O₂ was detected so early (8–48 s) by using a chemosensor. Although previous studies using boronate-based probes for H₂O₂ could detect endogenously produced H₂O₂, the timescale of the reaction was significantly longer (~20 min).³⁷ The use of a protein-based sensor for H₂O₂ revealed the rapid (within 1–2 min) generation of the ROS upon pharmacological stimulation;³⁸ our data matched theirs, validating the utility of selenide **1** for the biological studies of H₂O₂.

H₂O₂ has been highly recognized as a critical signaling agent for the recruitment of immune cells for wound regeneration.^{5-6, 9-10, 15, 39} In the zebrafish tail wounding model, we observed the rapid generation of H₂O₂ near the wound site. Our results here recapitulate the results observed by Niethammer *et al.*¹⁵ Importantly, we observed similar data using a small molecule probe that was previously observed using a protein-based sensor.¹⁵ Therefore, our study provides evidence that the previous imaging with genetically encoded HyPer protein is not an artifact due to the genetic manipulation.

Selenide **1** offers many advantages over currently available H₂O₂ probes. First is the obvious kinetic advantage; the probe reacts with a second order rate constant of $9.82 \pm 1.11 \text{ M}^{-1}\text{s}^{-1}$, while boronate-based probes react with a rate constant of about $1.3 \text{ M}^{-1} \text{ s}^{-1}$. Next, selenide **1** is highly selective for H₂O₂ over other ROS and

RNS. However, we acknowledge that two challenges exist with **1**. First, the cell permeability of the reporter fluorophore **5** leads to diffusion throughout the cell, complicating studies that require extended time periods. Second, the pK_a of phenol **5** is ~ 7 and thus would be pH sensitive under biological conditions. Nonetheless, the use of seleno Mislow-Evans rearrangement may provide a new platform for the design principle for fluorometric detection of intracellular H_2O_2 .

Acknowledgements

This work was funded by US National Science Foundation Grants CHE-0911092 and CHE-1506942. We thank Mr. Jevin M. Jupena (University of Pittsburgh) for the re-synthesis of probe **1**.

Experimental Methods

Fluorescence measurements and data analysis

All fluorescence measurements were taken on a Modulus II Microplate Multimode Reader (excitation 490 nm, emission 510-570 nm). Data analysis was performed using GraphPad Prism 6 or GraphPad Prism 7.

Reaction of 1 with H_2O_2

0–159 μM H_2O_2 in 5:95 MeCN/50 mM phosphate pH 7 buffer (180 μL) was added to the wells of a black 96-well plate. 100 μM **1** in MeCN (20 μL) was then added to the wells. The solutions were allowed to incubate at 25 °C for 20 min before the fluorescence was measured.

Determining selectivity of 1: Reaction with $O_2^{\bullet -}$

100 μM **1** in ethanol (20 μL) was added to 5:95 methanol/50 mM phosphate pH 7 buffer (140 μL). Then, either 0, 10, or 10^4 U/mL catalase (20 μL) was added to the mixtures. These solutions were transferred to centrifuge tubes containing solid potassium superoxide (~ 3 mg/sample). A control containing 100 μM **1** in ethanol (20 μL), 5:95 methanol/50 mM phosphate pH 7 buffer (160 μL), and 700 mM H_2O_2 (20 μL) was also generated. The solutions were allowed to incubate at 25 °C for 15 min prior to measuring fluorescence.

Determining selectivity of 1: Reaction with 1O_2

1 was titrated with $NaMoO_4$ and H_2O_2 to determine whether 1O_2 reacted with the probe. 100 μM **1** in ethanol (20 μL) was added to 5:95 methanol/50 mM phosphate pH 7 buffer (140 μL). Water, 1 mM sodium azide, or 10^4 U/mL catalase (20 μL) was added to the mixture. $NaMoO_4 \cdot 2H_2O$ (11.1 mg) was added to ultrapure water (2.00 mL). This solution was diluted to 20 μM , 200 μM , and 2.00 mM. H_2O_2 was diluted to 200 μM and 2.00 mM. Equal volumes of $NaMoO_4$ solution and H_2O_2 were added together and an aliquot (20 μL) was immediately transferred to the solution containing **1**. The fluorescence intensity was measured immediately and again after incubation at 25 °C for 40 min.

Determining selectivity of 1: Reaction with •OH

•OH was generated through the reaction of FeSO₄•7H₂O with H₂O₂. 100 μM **1** in ethanol (20 μL) was added to 5:95 methanol/50 mM phosphate pH 7 buffer (140 μL). Water or 10⁴ U/mL catalase (20 μL) was added to the mixture. FeSO₄•7H₂O (27.4 mg) was added to ultrapure water (2.00 mL). This solution was diluted to 20 μM, 200 μM, and 2.00 mM. H₂O₂ was diluted to 200 μM and 2.00 mM. Equal volumes of FeSO₄•7H₂O solution and H₂O₂ were added together and an aliquot (20 μL) was immediately transferred to the solution containing **1**. The fluorescence intensity was measured immediately and again after incubation at 25 °C for 40 min.

Determining selectivity of 1: Reaction with ClO⁻ and ONOO⁻

0, 1, 10, or 22 μM ONOO⁻ in 0.3 M NaOH (20 μL) or 1, 10, 100, or 1000 μM NaOCl in water (20 μL) was added to the wells of a black 96-well plate. A solution of 10 μM **1** in DMSO (560 μL) and 5:95 MeCN/1.2 M phosphate pH 7 buffer (4.48 mL) was made; this solution (180 μL) was transferred to each of the wells. The samples were allowed to incubate at 25 °C for 15 min before the fluorescence was measured.

Determining selectivity of 1: Reaction with ^tBuOOH

A solution of 5:95 MeCN/50 mM phosphate pH 7 buffer (160 μL) was added to the wells of a black 96-well plate. 10 μM **1** in DMSO (20 μL) was added to each well. 0 mM H₂O₂ in water (20 μL) or 0, 10, or 100 μM ^tBuOOH in DMSO (20 μL) were then added to the wells. The samples were allowed to incubate at 25 °C for 15 min before the fluorescence was measured.

Determining selectivity of 1: Reaction with NO₂⁻

NaNO₂ (97.0 mg) was dissolved in ultrapure water (2.00 mL). This solution was diluted to 10 μM, 100 μM, 1.00 mM, and 10.0 mM. H₂O₂ was diluted to 10 μM, 100 μM, 1.00 mM, and 10.0 mM. 100 μM **1** in ethanol (20 μL) was added to 5:95 methanol/50 mM phosphate pH 7 buffer (160 μL). The NaNO₂ or H₂O₂ solutions (20 μL) were added to the solution containing **1** and the fluorescence intensity was measured immediately and again after incubation at 25 °C for 15 min.

Determining selectivity of 1: Reaction with NO₃⁻

NaNO₃ (30.9 mg) was dissolved in ultrapure water (2.00 mL). This solution was diluted to 10 μM, 100 μM, 1.00 mM, and 10.0 mM. H₂O₂ was diluted to 10 μM, 100 μM, 1.00 mM, and 10.0 mM. 100 μM **1** in ethanol (20 μL) was added to 5:95 methanol/50 mM pH 7 potassium phosphate buffer (160 μL). The NaNO₃ or H₂O₂ solutions (20 μL) were added to the solution containing **1** and the fluorescence intensity was measured immediately and again after incubation at 25 °C for 15 min.

Determining selectivity of 1: Reaction with NO•

An NO• solution was generated by the addition of H₂SO₄ to NaNO₂. A round-bottom flask containing a saturated solution of NaNO₂ was connected to a series of three bubblers and one Erlenmeyer flask; the first two bubblers contained 30% NaOH, and the third contained ultrapure water. The flask contained ultrapure water (10

mL). The solutions were degassed with argon for 30 min. Then a 2 M solution of H₂SO₄ (1 mL) was added to the saturated NaNO₂ to produce a 1.8 mM solution of NO• (assuming saturation at 25 °C) in the flask. 10 μM **1** in DMSO (20 μL) was added to 5:95 acetonitrile/50 mM pH 7 potassium phosphate buffer (160 μL). The NO• solution (20 μL) was then added to the mixture containing **1**. The fluorescence was measured immediately and again after 15 min at 25 °C.

Cellular Imaging

Cells were seeded on 35-mm glass bottom dishes (MatTek Corporation, Ashland, MA) and incubated with 0.5 μM **1** for 15 min prior to imaging. In some cases, cells were incubated with 1 μM MitoTracker® Red FM (ThermoFisher Scientific) for 20 min at 37 °C. The treated cells were washed with HBSS, and the media was replaced with HBSS (2.00 mL). The dish was inserted in a closed, thermo-controlled (37 °C) stage top incubator (Tokai Hit Co., Shizuoka-ken, Japan) atop the motorized stage of an inverted Nikon TiE fluorescent microscope (Nikon Inc., Melville, NY) equipped with a 60X oil immersion optic (Nikon, CFI PlanFluor, NA 1.49) and NIS Elements Software. The sample was excited using the 470 nm line of a Lumencor diode-pumped light engine (SpectraX, Lumencor Inc., Beaverton OR). Fluorescence was detected using an ET-GFP filter set (Chroma Technology Corp) and ORCA-Flash 4.0 sCMOS camera (HAMAMATSU Corporation, Bridgewater, NJ). MitoTracker Red was excited using the 555 nm line and detected using a TRITC filter set. Data were collected every 30 s over a 10-min period.

Zebrafish tail-wounding model

Three-day post-fertilization zebrafish embryos were removed from their chorion and allowed to swim in 1 mM **1** for 2 h, leading to effective dye loading. Following this, the fish were anesthetized and mounted in agar. The tail fins were clipped with a razor blade. Fluorescence images were obtained every 60 s for 60 min using an inverted Nikon TiE fluorescent microscope (Nikon Inc., Melville, NY) equipped with a 20X 0.75 NA lens and NIS Elements Software. The sample was excited using the 470 nm line of a Lumencor diode-pumped light engine (SpectraX, Lumencor Inc., Beaverton OR), and the fluorescence signals were detected using an ET-GFP filter set (Chroma Technology Corp) and ORCA-Flash 4.0 sCMOS camera (HAMAMATSU Corporation, Bridgewater, NJ).

Mechanistic studies

Probe **1** (1.8 mg) was treated with CD₃OD (0.75 mL) and 943 mM H₂O₂ (1.9 μL). The crude reaction mixture was analyzed against known standards (**5** and acrolein). Figure S1 shows that both **5** and acrolein were formed during the reaction.

Methyl (E)-2-(6-((3-methoxy-3-oxoprop-1-en-1-yl)oxy)-3-oxo-3H-xanthen-9-yl)benzoate (8)

A suspension of **7**¹ (7.760 g, 22.52 mmol) in dry CH₂Cl₂ (390 mL) was treated with *N*-methylmorpholine (683 mg, 6.76 mmol) and methyl propiolate (9.467 mg, 112.6 mmol) under a nitrogen atmosphere at 23 °C. After stirring the reaction mixture for 24 h at the same temperature, silica gel (24 g) was added, and the mixture was concentrated *in vacuo*. The resulting crude residue was purified by flash column chromatography (10→90% EtOAc in hexanes) on silica gel (560 mL) to obtain vinyl ether **8** (7.65 g, 79%) as an orange solid. *Data for 8*: m.p.: 192.0–193.0 °C; R_f: 0.25 (70% EtOAc in hexanes); IR (film): ν_{max} = 3060, 2923, 1722 (C=O), 1642 (C=O), 1639 (C=O), 1595, 1522, 1444, 1378, 1267, 1247, 1191, 1158, 1133, 1106, 1081, 854, 707 cm⁻¹; ¹H NMR (300 MHz, CDCl₃, 293 K): δ 8.25 (dd, *J* = 7.5, 1.5 Hz, 1H), 7.85 (d, *J* = 12.0 Hz, 1H), 7.79 (ddd, *J* = 7.5, 7.5, 1.2 Hz, 1H), 7.72 (ddd, *J* = 7.5, 7.5, 1.2 Hz, 1H), 7.33 (dd, *J* = 7.5, 1.2 Hz, 1H), 7.18 (d, *J* = 2.4 Hz, 1H), 6.98 (d, *J* = 9.0 Hz, 1H), 6.89 (dd, *J* = 9.6, 1.8 Hz, 1H), 6.87 (d, *J* = 9.6 Hz, 1H), 6.56 (dd, *J* = 9.6, 1.8 Hz, 1H), 6.46 (d, *J* = 1.8 Hz, 1H), 5.79 (d, *J* = 12.0 Hz, 1H), 3.76 (s, 3H), 3.66 (s, 3H); ¹³C NMR (75 MHz, CDCl₃, 293 K): δ 185.9, 166.8, 165.5, 159.0, 158.5, 156.2, 153.4, 148.7, 134.3, 132.9, 131.3, 130.7, 130.6, 130.4, 130.2, 129.9, 129.3, 119.3, 118.1, 114.1, 106.4, 105.2, 104.8, 52.5, 51.6; HRMS (ESI-TOF) *m/z*: [M + H]⁺ calcd. for C₂₅H₁₉O₇ 431.1110, found 431.1125.

(*S,E*)-6'-((3-Hydroxyprop-1-en-1-yl)oxy)-3*H*-spiro[isobenzofuran-1,9'-xanthen]-3'-ol (9**)**

A 1 M solution of diisobutylaluminum hydride in hexanes (1.80 mL, 1.80 mmol) was added dropwise to a flask containing ester **8** (100 mg, 0.23 mmol) in dry CH₂Cl₂ (1.5 mL) under a nitrogen atmosphere at -78 °C. After stirring the reaction mixture for 15 min at the same temperature, the flask was warmed to 23 °C. The mixture was stirred at the same temperature for an additional 2 h, and then the reaction was quenched with 1 M aqueous sodium potassium tartrate (2 mL) at 0 °C. After stirring the mixture for 3 h at 23 °C, Et₂O (5 mL) and DDQ (57 mg, 0.25 mmol) were added at 0 °C and the resulting mixture was stirred at the same temperature for 1 h. The combined organic and aqueous layers were filtered through a pad of Celite, and the pad was rinsed with EtOAc. The filtrate was dried under Na₂SO₄, filtered through a cotton plug, and concentrated *in vacuo*. The resulting crude residue was purified by flash column chromatography (10→60% EtOAc in hexanes) on silica gel (20 mL) to obtain alcohol **9** (57 mg, 66%) as a pale yellow solid and byproduct **5** (14 mg, 20%) as an orange solid. *Data for 9*: m.p.: 169.0–170.0 °C; R_f: 0.52 (70% EtOAc in hexanes); IR (film): ν_{max} = 3378 (O–H), 2923, 2853, 1673, 1601, 1480, 1434, 1409, 1266, 1173, 1114, 1004, 926, 854, 722 cm⁻¹; ¹H NMR (300 MHz, 1% CD₃OD in CDCl₃, 293 K): δ 7.36–7.37 (m, 2H), 7.23–7.28 (m, 1H), 6.91 (d, *J* = 2.4 Hz, 1H), 6.88 (br s, 1H), 6.84 (d, *J* = 2.4 Hz, 1H), 6.77 (d, *J* = 8.4 Hz, 1H), 6.68–6.70 (m, 1H), 6.70 (dt, *J* = 12.0, 1.8 Hz, 1H), 6.60 (d, *J* = 2.4 Hz, 1H), 6.52 (dd, *J* = 8.7, 2.4 Hz, 1H), 5.57 (dt, *J* = 12.0*, 7.2 Hz, 1H), 5.29 (s, 2H), 4.15 (dd, *J* = 7.2, 1.8 Hz, 2H); ¹³C NMR (75 MHz, CD₃OD, 293 K): δ 154.0, 153.0, 149.6, 149.5, 143.9, 143.5, 138.6, 129.6, 129.1, 128.5, 128.4, 123.0, 120.9, 120.0, 118.0, 116.5, 116.4, 113.5, 104.5, 103.0, 83.0, 72.0, 58.0; HRMS (ESI-TOF) *m/z*: [M + H]⁺ calcd. for C₂₃H₁₉O₅ 375.1227, found 375.1209.

*It is typical for *trans* vinyl ethers to have *J* = 12.0 Hz coupling constant (see reference 2 for example)

(*S,E*)-6'-((3-(Phenylselanyl)prop-1-en-1-yl)oxy)-3*H*-spiro[isobenzofuran-1,9'-xanthen]-3'-ol (1)

A 10-mL round-bottomed flask equipped with a Teflon-coated magnetic stir bar containing **9** (85 mg, 0.23 mmol) was purged with argon. The flask was treated with THF (1.2 mL), ⁿBu₃P (67 μL, 0.27 mmol), and PhSeCN (29 μL, 0.23 mmol) sequentially at 0 °C. The mixture was stirred at the same temperature for 30 min and was then quenched with sat. NH₄Cl. The quenched mixture was extracted with EtOAc (3 × 15 mL). The combined organic layers were dried over Na₂SO₄ and concentrated *in vacuo*. The resulting crude residue was purified by flash column chromatography (SiO₂, eluent: 5%→25% EtOAc in hexanes; 30 mL each) to obtain **1** (48 mg, 41%) as pale-yellow solid. *Data for 1*: m.p.: 125.5–126.5 °C; R_f: 0.56 (40% EtOAc in hexanes); IR (film): ν_{max} = 3286 (broad, O-H), 2923, 2853, 2360, 1664, 1609, 1496, 1458, 1427, 1331, 1266, 1247, 1210, 1177, 1111, 997, 928, 846, 804, 757, 737, 691 cm⁻¹; ¹H NMR (300 MHz, 1% CD₃OD in CDCl₃, 293 K): δ 7.56 (dd, *J* = 6.0, 1.2 Hz, 2H), 7.36–7.34 (m, 2H), 7.32–7.31 (m, 3H), 7.27–7.26 (m, 1H), 6.88 (d, *J* = 7.5 Hz, 1H), 6.83 (dd, *J* = 8.1, 8.1 Hz, 2H), 6.66 (d, *J* = 2.4 Hz, 1H), 6.54 (m, 3H), 6.30 (d, *J* = 12.0 Hz, 1H), 5.57 (dt, *J* = 12.0, 8.4 Hz, 1H), 5.27 (s, 2H), 3.45 (dd, *J* = 8.1, 0.9 Hz, 2H); ¹³C NMR (75 MHz, CDCl₃, 293 K): δ 157.5, 156.5, 151.4, 151.3, 144.6, 143.1, 139.0, 134.4, 130.1, 130.0, 129.4, 129.2, 128.9, 128.4, 128.2, 127.7, 123.9, 120.7, 119.1, 117.0, 112.5, 111.8, 110.4, 103.6, 102.7, 83.6, 72.0, 25.6; HRMS (ESI-TOF) *m/z*: [M - H]⁺ calcd. for C₂₉H₂₁O₄Se 513.0610, found 513.0610.

REFERENCES

1. Winterbourn, C. C., Reconciling the Chemistry and Biology of Reactive Oxygen Species. *Nat. Chem. Biol.* **2008**, *4*, 278-286.
2. Simonian, N. A.; Coyle, J. T., Oxidative Stress in Neurodegenerative Diseases. *Annu. Rev. Pharmacol.* **1996**, *36*, 83-106.
3. Stone, J. R.; Yang, S., Hydrogen Peroxide: A Signaling Messenger. *Antiox. Redox. Sign.* **2006**, *8*, 243-270.
4. Dunnill, C.; Patton, T.; Brennan, J.; Barrett, J.; Dryden, M.; Cooke, J.; Leaper, D.; Georgopoulos, N. T., Reactive Oxygen Species (ROS) and Wound Healing: The Functional Role of ROS and Emerging ROS-Modulating Technologies for Augmentation of the Healing Process. *Int. Wound J.* **2017**, *14*, 89-96.
5. Hervera, A.; De Virgiliis, F.; Palmisano, I.; Zhou, L. M.; Tantardini, E.; Kong, G. P.; Hutson, T.; Danzi, M. C.; Perry, R. B.; Santos, C. X. C.; Kapustin, A. N.; Fleck, R. A.; Del Rio, J. A.; Carroll, T.; Lemmon, V.; Bixby, J. L.; Shah, A. M.; Fainzilber, M.; Di Giovanni, S., Reactive Oxygen Species Regulate Axonal Regeneration through the Release of Exosomal NADPH Oxidase 2 Complexes into Injured Axons. *Nat. Cell Biol.* **2018**, *20*, 307-319.
6. Jelcic, M.; Enyedi, B.; Xavier, J. B.; Niethammer, P., Image-Based Measurement of H₂O₂ Reaction Diffusion in Wounded Zebrafish Larvae. *Biophys. J.* **2017**, *112*, 2011-2018.
7. Kunkemoeller, B.; Kyriakides, T. R., Redox Signaling in Diabetic Wound Healing Regulates Extracellular Matrix Deposition. *Antiox. Redox. Sign.* **2017**, *27*, 823-838.
8. Martin, P.; Nunan, R., Cellular and Molecular Mechanisms of Repair in Acute and Chronic Wound Healing. *Brit. J. Dermatol.* **2015**, *173*, 370-378.
9. Niethammer, P., Wound Redox Gradients Revisited. *Semin. Cell Dev. Biol.* **2018**, *80*, 13-16.

10. Romero, M. M. G.; McCathie, G.; Jankun, P.; Roehl, H. H., Damage-Induced Reactive Oxygen Species Enable Zebrafish Tail Regeneration by Repositioning of Hedgehog Expressing Cells. *Nat. Commun.* **2018**, *9*.
11. Bliska, J. B.; Black, D. S., Inhibition of the Fc Receptor-Mediated Oxidativeburst in Macrophages by the Yersinia-Pseudotuberculosis Tyrosine Phosphatase. *Infect. Immun.* **1995**, *63*, 681-685.
12. Myhre, O.; Andersen, J. M.; Aarnes, H.; Fonnum, F., Evaluation of the Probes 2',7'-Dichlorofluorescein Diacetate, Luminol, and Lucigenin as Indicators of Reactive Species Formation. *Biochem. Pharmacol.* **2003**, *65*, 1575-1582.
13. Tarpey, M. M.; Fridovich, I., Methods of Detection of Vascular Reactive Species: Nitric Oxide, Superoxide, Hydrogen Peroxide, and Peroxynitrite. *Circ. Res.* **2001**, *89*, 224-236.
14. Levine, A.; Tenhaken, R.; Dixon, R.; Lamb, C., H₂O₂ from the Oxidative Burst Orchestrates the Plant Hypersensitive Disease Resistance Response. *Cell* **1994**, *79*, 583-593.
15. Niethammer, P.; Grabher, C.; Look, A. T.; Mitchison, T. J., A Tissue-Scale Gradient of Hydrogen Peroxide Mediates Rapid Wound Detection in Zebrafish. *Nature* **2009**, *459*, 996-999.
16. Markvicheva, K. N.; Bilan, D. S.; Mishina, N. M.; Gorokhovatsky, A. Y.; Vinokurov, L. M.; Lukyanov, S.; Belousov, V. V., A Genetically Encoded Sensor for H₂O₂ with Expanded Dynamic Range. *Bioorg. Med. Chem.* **2011**, *19*, 1079-1084.
17. Dickinson, B. C.; Tang, Y.; Chang, Z. Y.; Chang, C. J., A Nuclear-Localized Fluorescent Hydrogen Peroxide Probe for Monitoring Sirtuin-Mediated Oxidative Stress Responses in Vivo. *Chem. Biol.* **2011**, *18*, 943-948.
18. Chang, M. C. Y.; Pralle, A.; Isacoff, E. Y.; Chang, C. J., A Selective, Cell-Permeable Optical Probe for Hydrogen Peroxide in Living Cells. *J. Am. Chem. Soc.* **2004**, *126*, 15392-15393.
19. Wang, H.; He, Z.; Yang, Y.; Zhang, J.; Zhang, W.; Zhang, W.; Li, P.; Tang, B., Ratiometric Fluorescence Imaging of Golgi H₂O₂ Reveals a Correlation between Golgi Oxidative Stress and Hypertension. *Chem. Sci.* **2019**, *10*, 10876-10880.
20. Zheng, D. J.; Yang, Y. S.; Zhu, H. L., Recent Progress in the Development of Small-Molecule Fluorescent Probes for the Detection of Hydrogen Peroxide. *Trac-Trend Anal. Chem.* **2019**, *118*, 625-651.
21. Pallu, J.; Rabin, C.; Creste, G.; Branca, M.; Mavre, F.; Limoges, B., Exponential Molecular Amplification by H₂O₂-Mediated Autocatalytic Deprotection of Boronic Ester Probes to Redox Cyclers. *Chem.-Eur. J.* **2019**, *25*, 7534-7546.
22. Evans, D. A.; Andrews, G. C., Allylic Sulfoxides - Useful Intermediates in Organic Synthesis. *Acc. Chem. Res.* **1974**, *7*, 147-155.
23. Reich, H. J., Organoselenium Chemistry - Synthetic Transformations Based on Allyl Selenide Anions. *J. Org. Chem.* **1975**, *40*, 2570-2572.
24. Albert, B. J.; Sivaramakrishnan, A.; Naka, T.; Czaicki, N. L.; Koide, K., Total Syntheses, Fragmentation Studies, and Antitumor/Antiproliferative Activities of FR901464 and Its Low Picomolar Analogue. *J. Am. Chem. Soc.* **2007**, *129*, 2648-2659.
25. Grieco, P. A.; Gilman, S.; Nishizawa, M., Organoselenium Chemistry - Facile One-Step Synthesis of Alkyl Aryl Selenides from Alcohols. *J. Org. Chem.* **1976**, *41*, 1485-1486.
26. Krief, A.; Lonez, F., Singlet Oxygen Oxidation of Selenides to Selenoxides. *Tetrahedron Lett.* **2002**, *43*, 6255-6257.
27. Ando, S.; Koide, K., Development and Applications of Fluorogenic Probes for Mercury(II) Based on Vinyl Ether Oxymercuration. *J. Am. Chem. Soc.* **2011**, *133*, 2556-2566.

28. Chen, G. W.; Song, F. L.; Wang, J. Y.; Yang, Z. G.; Sun, S. G.; Fan, J. L.; Qiang, X. X.; Wang, X.; Dou, B. R.; Peng, X. J., FRET Spectral Unmixing: A Ratiometric Fluorescent Nanoprobe for Hypochlorite. *Chem. Commun.* **2012**, *48*, 2949-2951.
29. Osada, M.; Ogura, Y.; Yasui, H.; Sakurai, H., Involvement of Singlet Oxygen in Cytochrome P450-Dependent Substrate Oxidations. *Biochem. Biophys. Res. Co.* **1999**, *263*, 392-397.
30. Yamada, K.; Ono, T.; Nishioka, H., Effect of Nan₃ on Oxygen-Dependent Lethality of UV-A in Escherichia Coli Mutants Lacking Active Oxygen-Defense and DNA-Repair Systems. *J. Radiat. Res.* **1996**, *37*, 29-37.
31. Miller, E. W.; Albers, A. E.; Pralle, A.; Isacoff, E. Y.; Chang, C. J., Boronate-Based Fluorescent Probes for Imaging Cellular Hydrogen Peroxide. *J. Am. Chem. Soc.* **2005**, *127*, 16652-16659.
32. Swindle, E. J.; Hunt, J. A.; Coleman, J. W., A Comparison of Reactive Oxygen Species Generation by Rat Peritoneal Macrophages and Mast Cells Using the Highly Sensitive Real-Time Chemiluminescent Probe Pholasin: Inhibition of Antigen-Induced Mast Cell Degranulation by Macrophage-Derived Hydrogen Peroxide. *J. Immunol.* **2002**, *169*, 5866-5873.
33. Advanced Organic Chemistry: Reaction Mechanisms By Reinhard Bruckner, 1st edition, Page 573 Chapter 14
34. Chang, C. Y.; Hsieh, Y. H.; Cheng, K. Y.; Hsieh, L. L.; Cheng, T. C.; Yao, K. S., Effect of pH on Fenton Process Using Estimation of Hydroxyl Radical with Salicylic Acid as Trapping Reagent. *Water Sci. Technol.* **2008**, *58*, 873-879.
35. Merenyi, G.; Lind, J.; Czapski, G.; Goldstein, S., The Decomposition of Peroxynitrite Does Not Yield Nitroxyl Anion and Singlet Oxygen. *Proc. Natl. Acad. Sci. U.S.A.* **2000**, *97*, 8216-8218.
36. Beckman, J. S.; Beckman, T. W.; Chen, J.; Marshall, P. A.; Freeman, B. A., Apparent Hydroxyl Radical Production by Peroxynitrite - Implications for Endothelial Injury from Nitric-Oxide and Superoxide. *Proc. Natl. Acad. Sci. U.S.A.* **1990**, *87*, 1620-1624.
37. Rodella, U.; Scorzeto, M.; Duregotti, E.; Negro, S.; Dickinson, B. C.; Chang, C. J.; Yuki, N.; Rigoni, M.; Montecucco, C., An Animal Model of Miller Fisher Syndrome: Mitochondrial Hydrogen Peroxide Is Produced by the Autoimmune Attack of Nerve Terminals and Activates Schwann Cells. *Neurobiol. Dis.* **2016**, *96*, 95-104.
38. Ermakova, Y. G.; Bilan, D. S.; Matlashov, M. E.; Mishina, N. M.; Markvicheva, K. N.; Subach, O. M.; Subach, F. V.; Bogeski, I.; Hoth, M.; Enikolopov, G.; Belousov, V. V., Red Fluorescent Genetically Encoded Indicator for Intracellular Hydrogen Peroxide. *Nat. Commun.* **2014**, *5*, 5222.
39. Enyedi, B. N., P., H₂O₂: A Chemoattractant? In *Methods Enzymol.*, Cadenas, E. P., L., Ed. 2013; Vol. 528, pp 237-255.

Supplementary Information

for

Fluorogenic Probe Using a Mislow-Evans Rearrangement for Time-Resolved Imaging of Hydrogen Peroxide

Dianne Pham¹, Upamanyu Basu¹, Ivanna Pohorilets¹, Claudette M. St Croix², Simon C. Watkins², and Kazunori Koide^{1*}

¹Department of Chemistry, University of Pittsburgh, 219 Parkman Avenue, Pittsburgh, Pennsylvania 15260, United States

²Center for Biologic Imaging, Department of Cell Biology, University of Pittsburgh, 3500 Terrace Street, Pittsburgh, Pennsylvania 15261, United States

koide@pitt.edu

General Techniques

All reactions were carried out with freshly distilled solvents under anhydrous conditions, unless otherwise noted. All of the flasks used for carrying out reactions were dried in an oven at 80 °C prior to use. Unless specifically stated, the temperature of a water bath during the evaporation of organic solvents using a rotary evaporator was about 35 ± 5 °C. All of the syringes in this study were dried in an oven at 80 °C and stored in a desiccator over Drierite®. Tetrahydrofuran (THF) was distilled over sodium metal and benzophenone. Methylene chloride (CH₂Cl₂) was distilled over calcium hydride. Acetonitrile was distilled from CaH₂ and stored over 3 Å molecular sieves. Yields refer to chromatographically and spectroscopically (¹H NMR) homogenous materials, unless otherwise stated. All reactions were monitored by thin-layer chromatography (TLC) carried out on 0.25-mm Merck silica gel plates (60F-254) using UV light (254 nm) for visualization or anisaldehyde in ethanol or 2.4% phosphomolybdic acid/1.4% phosphoric acid/5% sulfuric acid in water as a developing agents and heat for visualization. Silica gel (230–400 mesh) was used for flash column chromatography. A rotary evaporator was connected to a water aspirator that produced a vacuum pressure of approximately 60 mmHg when it was connected to the evaporator. NMR spectra were recorded on a Bruker Advance spectrometer at 300 MHz, 400 MHz, 500 MHz, 600 MHz or 700 MHz. The chemical shifts are given in parts per million (ppm) on a delta (δ) scale. The solvent peak was used as a reference value: for ¹H NMR: CHCl₃ = 7.27 ppm, CH₃OH = 3.31 ppm, CH₃CN = 2.08 ppm; for ¹³C NMR: CDCl₃ = 77.00 ppm, CD₃OD = 49.00 ppm, and CD₃CN = 1.79 ppm for CD₃ or 118.26 ppm for CN. The following abbreviations are used to indicate the multiplicities: s = singlet; d = doublet; t = triplet; q = quartet; m = multiplet; br = broad. High-resolution mass spectra were recorded on a VG 7070 spectrometer. Low-resolution mass spectra [LCMS (ESI)] were recorded on a Shimadzu LCMS-2020. Infrared (IR) spectra were collected on a Mattson Cygnus 100 spectrometer. Samples for acquiring IR spectra were prepared as a thin film on a NaCl plate by dissolving the compound in CH₂Cl₂ and then evaporating the CH₂Cl₂.

All fluorescence measurements (excitation 490 nm, emission 510–570 nm) were carried out using a Promega Biosystems Modulus II Microplate Reader or a HoribaMax Fluorometer.

HPLC chromatogram of selenide 1 and phenoxide 5

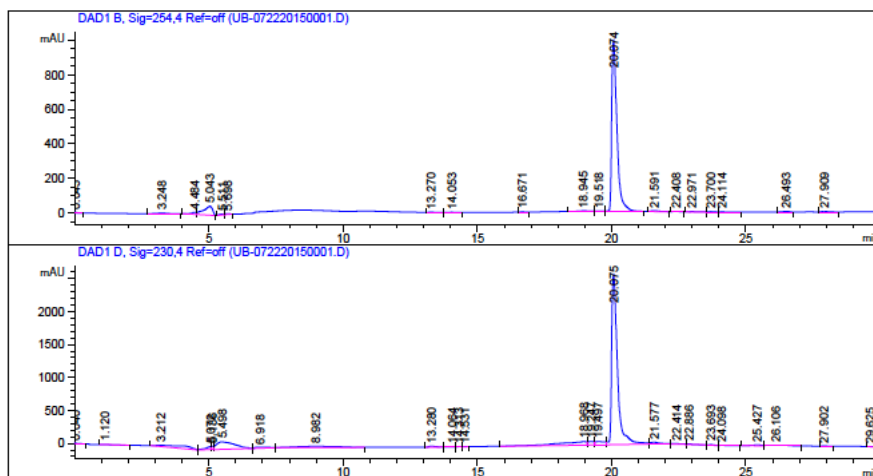
Column: Agilent 1200 system; Flow rate: 0.6 mL/min; Max. Pressure (bar): 600

Elution conditions: H₂O/MeCN 95:5 to 20:80, 0–15 min; 20:80 to 0:100, 15–20 min; 0:100, 20–25 min; 0:100 to 95:5, 25–30 min

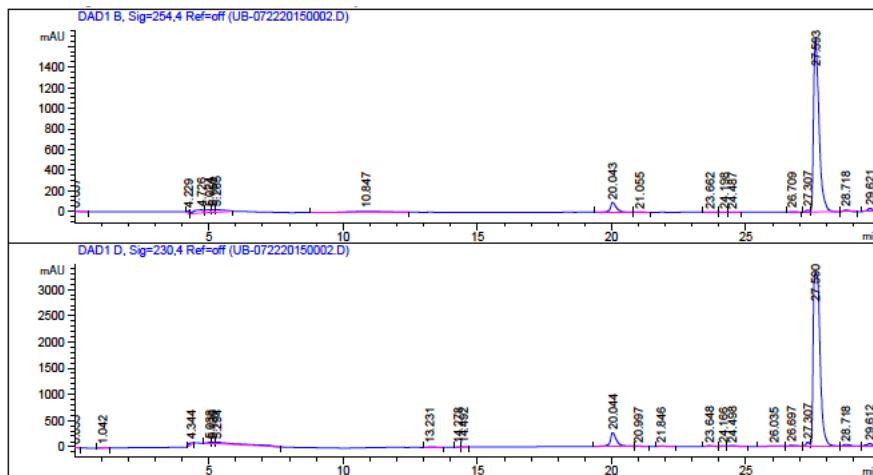
Retention time for **1**: 20.1 min

Retention time for **5**: 27.6 min

(a)



(b)



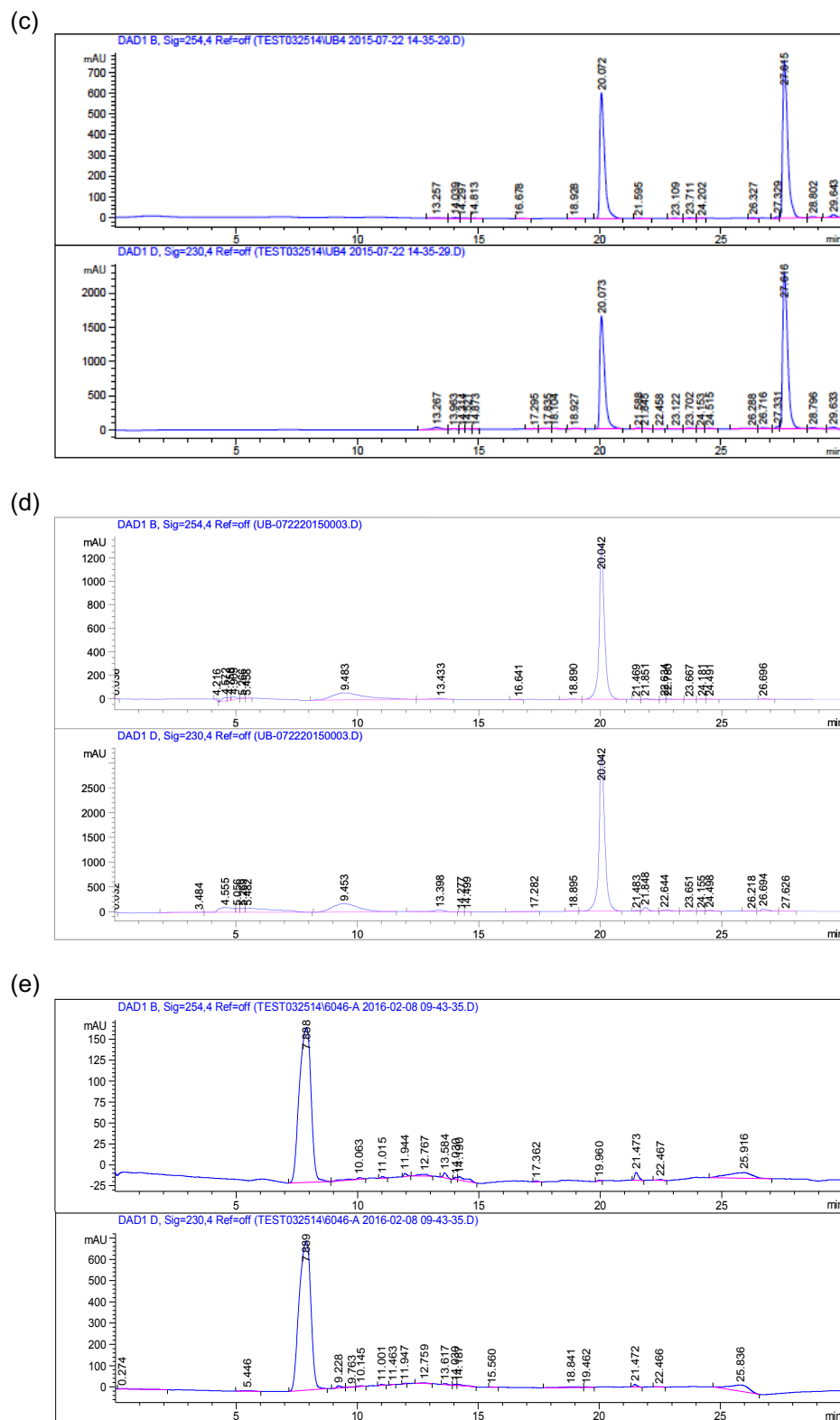
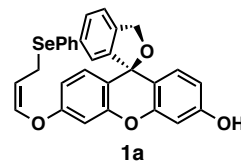
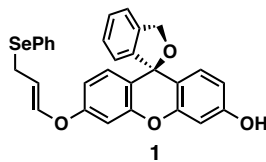


Figure S1. HPLC chromatograms of (a) authentic sample of selenide **1** (b) phenol **5** (c) selenide **1** + phenol **5** (d) crude reaction mixture of selenide **1** + 1 equiv H₂O₂, and (e) authentic sample of PhSeO₂H acquired at $\lambda = 254$ nm and 230 nm, respectively.

Stability studies

To study the stability of **1**, the ^1H NMR spectra of **1** in $\text{DMSO-}d_6$ was recorded at specified intervals (days 1, 7, 14, 21, 30 and 60) while the solution was left at room temperature and in air throughout the entire period.



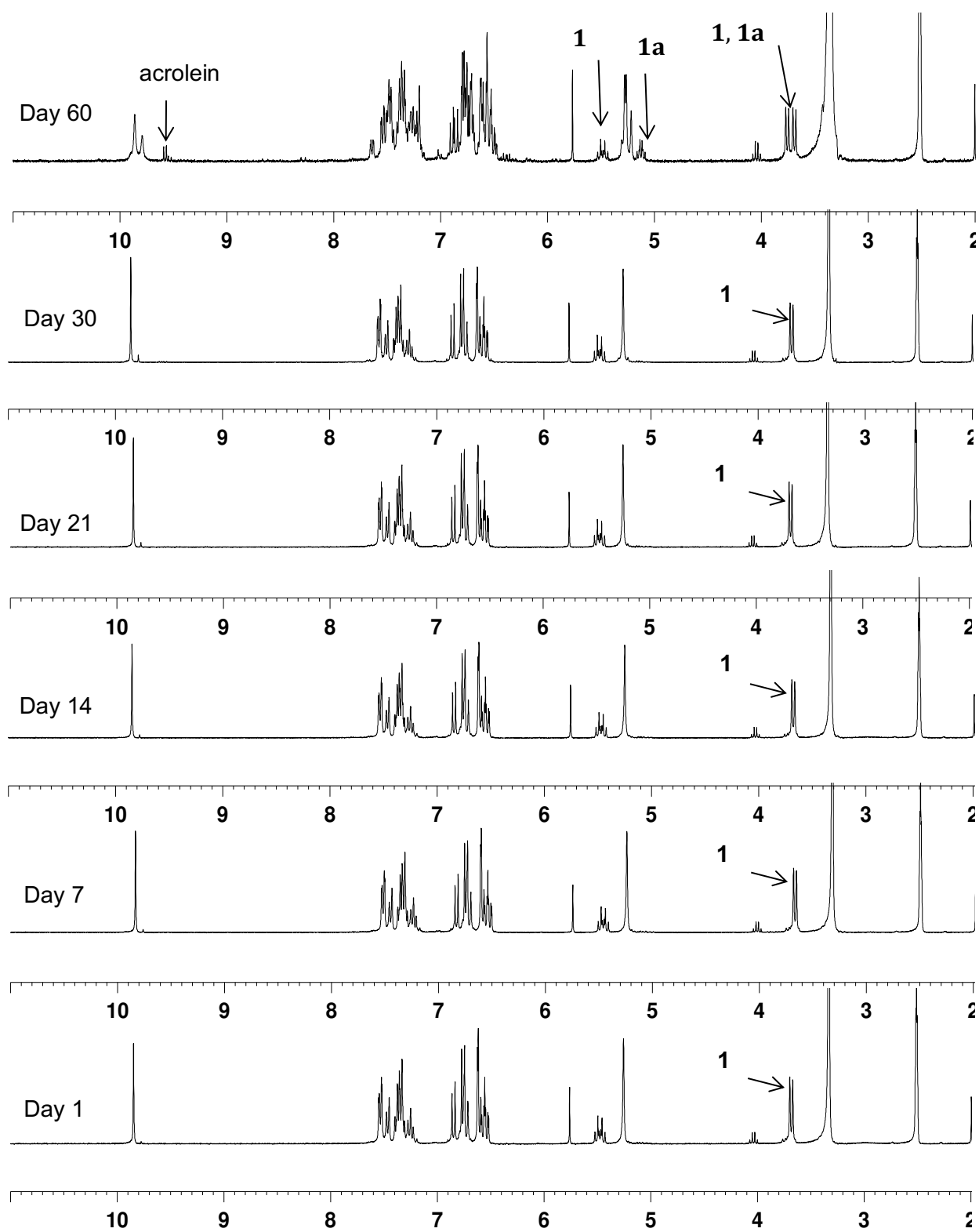
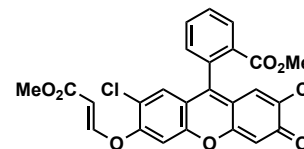


Figure S2. ¹H NMR spectra (300 MHz, DMSO-*d*₆) of **1** recorded on days 1, 7, 14, 21, 30 and 60.

The following compounds were synthesized following the general procedure described in the main text.

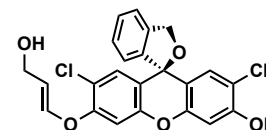
Methyl (*E*)-2-(2,7-dichloro-6-((3-methoxy-3-oxoprop-1-en-1-yl)oxy)-3-oxo-3*H*-xanthen-9-yl)benzoate (S2**)**



Data for S2: Yield: 17% (orange solid); m.p.: 202.0–203.0 °C; R_f : 0.20 (40% EtOAc in hexanes); IR (film): ν_{\max} = 3065, 2951, 1719, 1652, 1625, 1592, 1525, 1433,

1336, 1273, 1236, 1173, 1111, 1084, 1041, 998 cm^{-1} ; ^1H NMR (300 MHz, CDCl_3 , 293 K): δ 8.37 (dd, $J=7.8$, 1.2 Hz, 1H), 7.87–7.75 (m, 2H), 7.77 (d, $J=12.0$ Hz, 1H), 7.34 (dd, $J=7.8$, 1.2 Hz, 1H), 7.03 (s, 1H), 6.98 (s, 1H), 6.62 (s, 1H), 5.84 (d, $J=12.0$ Hz, 1H), 3.79 (s, 3H), 3.74 (s, 3H); ^{13}C NMR (100 MHz, CD_3OD , 293 K): δ 178.0, 166.4, 165.2, 157.5, 155.9, 154.5, 151.4, 148.5, 136.1, 133.5, 133.4, 131.7, 130.5, 130.4, 129.8, 128.8, 127.3, 121.1, 119.3, 118.6, 106.5, 106.3, 105.8, 52.7, 51.8; HRMS (ESI-TOF) m/z : $[\text{M} + \text{H}]^+$ calcd. for $\text{C}_{25}\text{H}_{17}\text{Cl}_2\text{O}_7$ 499.0346, found 499.0331.

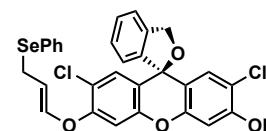
(*S,E*)-2',7'-Dichloro-6'-((3-hydroxyprop-1-en-1-yl)oxy)-3*H*-spiro[isobenzofuran-1,9'-xanthen]-3'-ol (S3**)**



Data for S3: Yield: 58% (yellow solid); m.p.: 204.2–205.0 °C; R_f : 0.26 (60% EtOAc in

hexanes); IR (film): ν_{\max} = 3378, 2921, 2851, 1673, 1601, 1480, 1434, 1409, 1266, 1173, 1114, 1004, 922, 864, 722 cm^{-1} ; ^1H NMR (300 MHz, CD_3OD , 293 K): δ 7.53 (s, 1H), 7.417.40 (m, 2H), 7.33–7.27 (m, 1H), 6.93 (s, 1H), 6.89 (s, 1H), 6.86 (d, $J=7.5$ Hz, 1H), 6.81 (s, 1H), 6.74 (s, 1H), 6.69 (d, $J=12.0$ Hz, 1H), 5.64 (dt, $J=12.0$, 6.9 Hz, 1H), 5.29 (s, 2H), 4.13 (d, $J=6.9$ Hz, 1H); ^{13}C NMR (75 MHz, CD_3OD , 293 K): δ 154.0, 152.9, 149.6, 149.5, 143.9, 143.5, 138.6, 129.6, 129.1, 128.5, 128.4, 123.0, 120.9, 120.1, 118.0, 116.5, 116.4, 113.5, 104.5, 103.0, 83.0, 72.0, 58.0; HRMS (ESI-TOF) m/z : $[\text{M} + \text{H}]^+$ calcd. for $\text{C}_{23}\text{H}_{17}\text{Cl}_2\text{O}_5$ 443.0448, found 443.0450.

(*S,E*)-2',7'-Dichloro-6'-((3-(phenylselanyl)prop-1-en-1-yl)oxy)-3*H*-spiro[isobenzofuran-1,9'-xanthen]-3'-ol (S4**)**



Data for S4: Yield: 27% (yellow foam); R_f : 0.30 (20% EtOAc in hexanes); IR (film):

ν_{\max} = 3242 (O-H), 2917, 1664, 1625, 1605, 1479, 1435, 1409, 1350, 1266, 1245, 1174, 1107, 1024, 874, 734 cm^{-1} ; ^1H NMR (300 MHz, CD_3CN , 293 K): δ 7.54–7.51 (m, 3H), 7.40–7.32 (m, 5H), 6.91 (s, 1H), 6.88 (s, 1H), 6.82 (s, 1H), 6.38 (s, 1H), 6.38 (br d, $J=12.0$ Hz, 1H), 5.58 (dt, $J=12.0$, 8.4 Hz, 1H), 5.29 (s, 1H), 3.57 (dd, $J=8.4$, 0.9 Hz, 2H); ^{13}C NMR (150 MHz, CD_3CN , 293 K): δ 154.1, 153.7, 150.2, 150.1, 145.6, 143.3, 139.5, 134.7, 130.6, 130.5, 130.3, 130.2, 130.1, 129.6, 129.5, 128.6, 124.0, 122.4, 121.4, 118.9, 117.0, 113.4, 105.2, 104.6, 83.3, 79.1, 73.6, 25.0; HRMS (ESI-TOF) m/z : $[\text{M} - \text{H}]^+$ calcd. for $\text{C}_{29}\text{H}_{19}\text{Cl}_2\text{O}_4\text{Se}$ 580.9820, found 580.9826.

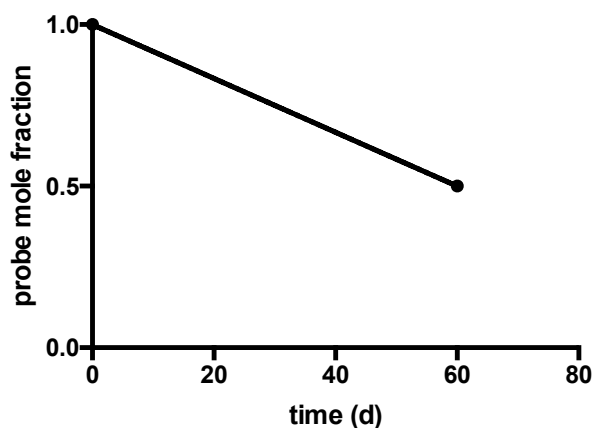


Figure S3. Half-life of probe 1.

Determination of the difference in fluorescence intensity between selenide 1 and phenol 5

Solutions containing ultrapure water (681 μL), 1.2 M phosphate pH 7 buffer (31 μL), DMSO (28.1 μL), and 80 μM **1** or phenol **5** in DMSO (9.4 μL) were made. Aliquots of these solutions (200 μL) were transferred to the wells of a black 96-well plate and the fluorescence was measured.

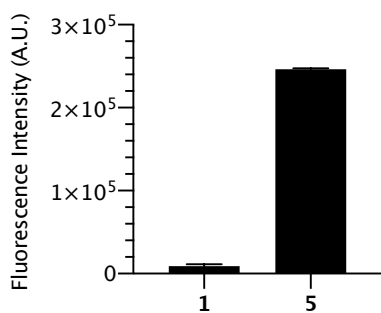


Figure S4. Difference in fluorescence intensity between selenide **1** and phenol **5**.

Compound	Fluorescence Intensity		
1	7,053	11,524	8,556
5	244,687	247,204	246,848

Table S1. Raw fluorescence values for Figure S4. $n = 3$.

Pseudo first order kinetics and evaluation of second order rate constant

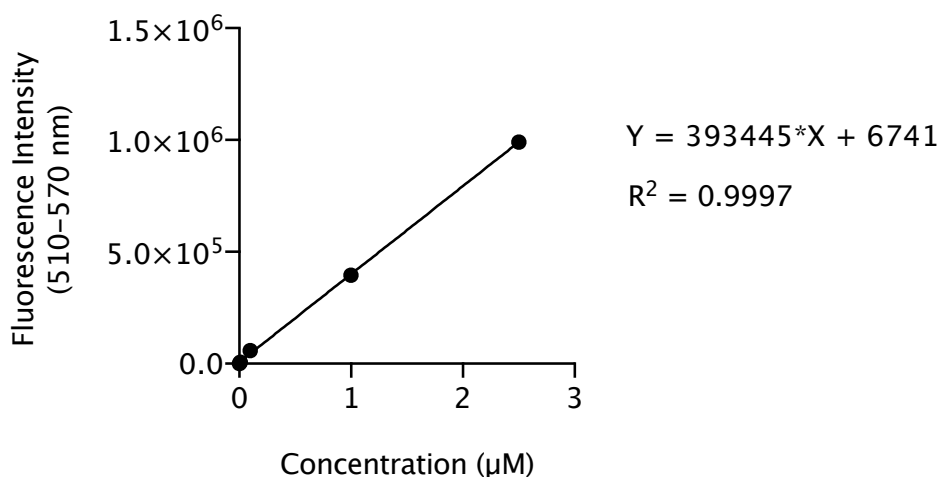


Figure S5. Calibration curve for phenol **5**: Volume: 200 μL , 5% MeCN in 50 mM pH 7.5 HEPES buffer.

$F_0 = 24616$ units

Time (s)	F-F ₀ (515 nm); [H ₂ O ₂] = 0.625 mM			F-F ₀ (515 nm); [H ₂ O ₂] = 1.25 mM			F-F ₀ (515 nm); [H ₂ O ₂] = 2.5 mM		
	Expt. 1	Expt. 2	Expt. 3	Expt. 1	Expt. 2	Expt. 3	Expt. 1	Expt. 2	Expt. 3
30	145,691	101,161	83,026	255,659	258,915	225,047	425,024	405,551	398,309
90	220,196	277,036	236,883	364,712	517,271	484,926	539,467	612,814	630,136
150	301,900	391,059	348,470	463,364	607,290	590,662	601,940	657,981	671,943
210	355,049	458,596	422,910	514,663	641,798	639,332	627,168	666,435	680,181
270	390,358	499,861	473,964	549,297	656,229	660,178	636,230	665,190	679,336
330	421,561	522,358	509,584	572,635	661,539	664,254	638,753	666,173	674,138
390	450,025	534,705	536,252	589,797	665,178	666,753	641,141	663,899	664,993
450	477,638	541,922	555,207	601,493	663,842	669,367	640,270	661,893	664,413
510	501,767	546,290	569,868	606,377	663,608	673,539	639,383	659,509	664,003
570	524,121	550,122	581,518	612,207	662,594	675,671	637,346	658,746	663,104
630	543,908	551,490	591,076	614,405	663,947	677,477	637,422	656,826	661,222
690	559,985	551,741	599,176	616,203	663,123	679,640	636,174	654,911	659,002
750	570,897	553,475	603,780	616,371	663,595	679,888	634,294	654,494	657,410
810	580,693	553,568	609,902	614,783	663,765	683,016	631,953	653,606	654,988
870	587,536	552,326	614,108	614,819	662,173	685,799	631,346	651,140	655,338

Table S2. Raw data for Figure 4a.

Raw data for studying pseudo first order kinetics

Rate= $k'[1]$; where $k' = k[H_2O_2]$

Final concentration: $[H_2O_2] = 0.625$ mM, 1.25 mM and 2.5 mM; $[1] = 1.7$ μ M; 5% MeCN in pH 7.5 HEPES buffer 50 mM. All reactions were performed in triplicate in a 96-well plate.

Calculating $[1]$ from the standard curve of **5**. Fluorescence Intensity = $393445 \cdot [5] + 6741$; $R^2 = 0.9997$.

Time (s)	$[1]$ μ M $[H_2O_2] = 0.625$ mM			$[1]$ μ M $[H_2O_2] = 1.25$ mM			$[1]$ μ M $[H_2O_2] = 2.5$ mM		
	Exp. 1	Exp. 2	Exp. 3	Exp. 1	Exp. 2	Exp. 3	Exp. 1	Exp. 2	Exp. 3
30	1.3453	1.4596	1.5061	1.0631	1.0547	1.1417	0.6285	0.6785	0.6971
90	1.1541	1.0082	1.1113	0.7833	0.3918	0.4748	0.3348	0.1466	0.1022
150	0.9444	0.7157	0.8249	0.5301	0.1608	0.2035	0.1745	0.0307	-0.005
210	0.8081	0.5424	0.6339	0.3985	0.0722	0.0786	0.1098	0.0090	-0.026
270	0.7175	0.4365	0.5029	0.3096	0.0352	0.0251	0.0865	0.0122	-0.024
330	0.6374	0.3787	0.4115	0.2497	0.0216	0.0146	0.0801	0.0097	-0.010
390	0.5643	0.3470	0.3431	0.2057	0.0122	0.0082	0.0739	0.0155	0.0127
450	0.4935	0.3285	0.2944	0.1757	0.0157	0.0015	0.0762	0.0207	0.0142
510	0.4316	0.3173	0.2568	0.1631	0.0163	-0.009	0.0784	0.0268	0.0153
570	0.3742	0.3075	0.2269	0.1482	0.0189	-0.014	0.0837	0.0288	0.0176
630	0.3234	0.3040	0.2024	0.1425	0.0154	-0.019	0.0835	0.0337	0.0224
690	0.2822	0.3033	0.1816	0.1379	0.0175	-0.024	0.0867	0.0386	0.0281
750	0.2542	0.2989	0.1698	0.1375	0.0163	-0.025	0.0915	0.0397	0.0322
810	0.2290	0.2986	0.1541	0.1416	0.0159	-0.033	0.0975	0.0419	0.0384
870	0.2115	0.3018	0.1433	0.1415	0.0200	-0.040	0.0991	0.0483	0.0375

Table S3. Raw data for Figure 4b.

$[H_2O_2]$ (mM)	Slope k' (s^{-1})
2.5	0.02432
1.25	0.01359
0.625	0.00251

Table S4. Slope (k') obtained from the plot of $\ln [1]$ vs time.

From Figure 3b, three values of k' were obtained for three different concentrations of H_2O_2 . Under pseudo first order conditions, $k' = k[H_2O_2]$. So, a plot of observed rate constant k' vs $[H_2O_2]$ yielded the second order rate constant k as the slope of the linear plot. After all calculations, it was found that second order rate constant $k = 9.82 \pm 1.11$ $M^{-1}s^{-1}$.

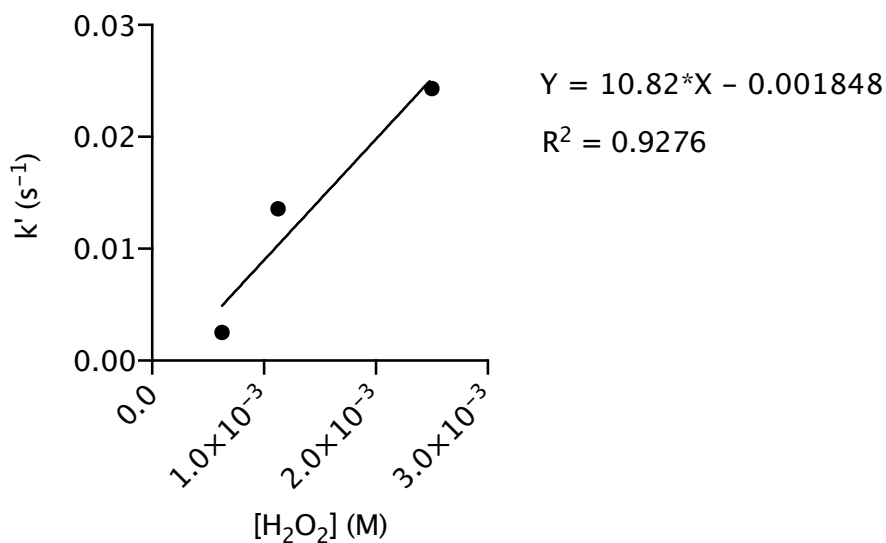


Figure S6. Plot of k' vs time to obtain second order rate constant k .

Similarly, the second order rate constant for **S4** was also calculated from the following plots.

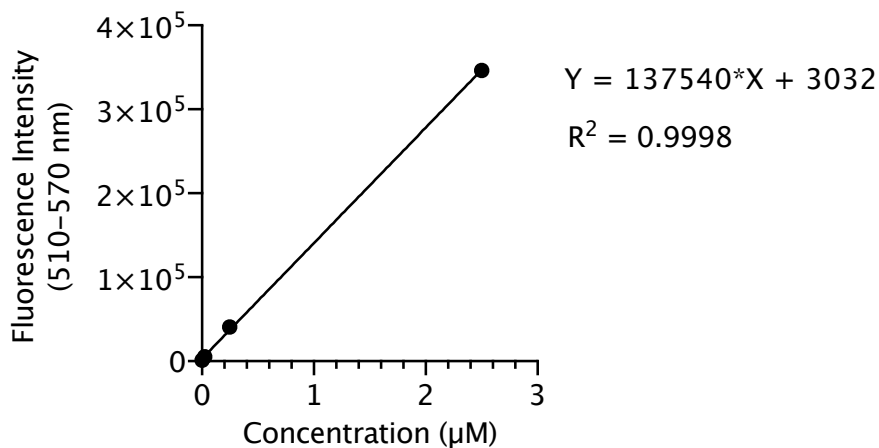


Figure S7. Calibration curve for Pittsburgh Green: 200 μL, 5% MeCN in 50 mM pH 7.5 HEPES buffer

$F_0 = 974.222$ arbitrary units (before addition of H_2O_2)

[Probe] = 2.5 μM

[H_2O_2] = 250, 125, 62.5 μM, respectively

Time (s)	F-F ₀ (515 nm); [H ₂ O ₂] = 62.5 μM			F-F ₀ (515 nm); [H ₂ O ₂] = 125 μM			F-F ₀ (515 nm); [H ₂ O ₂] = 250 μM		
	Expt. 1	Expt. 2	Expt. 3	Expt. 1	Expt. 2	Expt. 3	Expt.1	Expt. 2	Expt. 3
30	64,532	60,839	72,341	51,068	40,954	29,407	20,933	20,713	17,895
90	94,055	84,890	99,777	61,620	54,853	38,434	26,549	26,261	22,833
150	126,168	110,059	125,746	75,450	68,745	48,938	32,203	32,013	27,511
210	151,144	132,904	151,809	88,218	82,399	59,492	38,434	38,112	32,023
270	174,202	154,143	173,840	99,254	94,711	69,782	45,581	45,714	38,555
330	195,425	176,762	196,268	110,291	106,912	80,261	54,391	53,856	46,349
390	214,125	195,309	213,903	120,534	118,426	90,136	61,465	61,141	55,115
450	235,080	213,946	228,931	132,699	129,729	101,653	68,335	68,705	62,745
510	251,284	232,113	245,365	142,828	140,659	113,203	74,962	76,129	70,760
570	267,145	247,451	259,690	152,548	149,939	120,429	82,980	83,409	78,331
630	277,115	262,327	273,899	163,508	160,682	132,151	89,955	91,138	85,442
690	280,646	276,049	285,043	174,252	170,447	142,735	98,437	100,429	95,200
750	285,014	290,726	296,951	184,048	179,818	153,582	105,665	107,760	102,828
810	291,608	306,540	310,230	193,989	188,931	160,835	113,559	114,196	111,796
870	298,779	319,772	321,793	203,331	197,010	172,486	119,974	121,528	117,097

Table S5. Raw data for calculation of pseudo 1st order rate constant for **S4**.

Calculation of [S4] from observed fluorescence values and standard curve of Pittsburgh Green:

Time (s)	[S4] [H ₂ O ₂] = 62.5 μM			[S4] [H ₂ O ₂] = 125 μM			[S4] [H ₂ O ₂] = 250 μM		
	Expt. 1	Expt. 2	Expt. 3	Expt. 1	Expt. 2	Expt. 3	Expt. 1	Expt. 2	Expt. 3
30	2.0527	2.0795	1.9959	2.1506	2.1946	2.3081	2.3698	2.3714	2.3919
90	1.8380	1.9046	1.7963	2.0739	2.0826	2.2425	2.3289	2.3310	2.3559
150	1.6044	1.7216	1.6075	1.9733	1.9707	2.1661	2.2878	2.2892	2.3219
210	1.4228	1.5554	1.4179	1.8804	1.8608	2.0893	2.2425	2.2448	2.2891
270	1.2551	1.4010	1.2577	1.8002	1.7616	2.0145	2.1905	2.1895	2.2416
330	1.1007	1.2365	1.0946	1.7199	1.6634	1.9383	2.1264	2.1303	2.1849
390	0.9647	1.1016	0.9663	1.6454	1.5707	1.8665	2.0750	2.0773	2.1212
450	0.8123	0.9660	0.8570	1.5569	1.4796	1.7827	2.0250	2.0223	2.0657
510	0.6945	0.8339	0.7375	1.4832	1.3916	1.6987	1.9768	1.9683	2.0074
570	0.5791	0.7224	0.6333	1.4126	1.3169	1.6461	1.9185	1.9154	1.9523
630	0.5066	0.6142	0.5300	1.3329	1.2304	1.5609	1.8678	1.8592	1.9006
690	0.4809	0.5144	0.4490	1.2547	1.1517	1.4839	1.8061	1.7916	1.8296
750	0.4492	0.4076	0.3624	1.1835	1.0763	1.4050	1.7535	1.7383	1.7742
810	0.4012	0.2926	0.2658	1.1112	1.0029	1.3523	1.6961	1.6915	1.7089
870	0.3491	0.1964	0.1817	1.0432	0.9378	1.2676	1.6495	1.6382	1.6704

Table S6. Raw data for calculation of [S4] (μM).

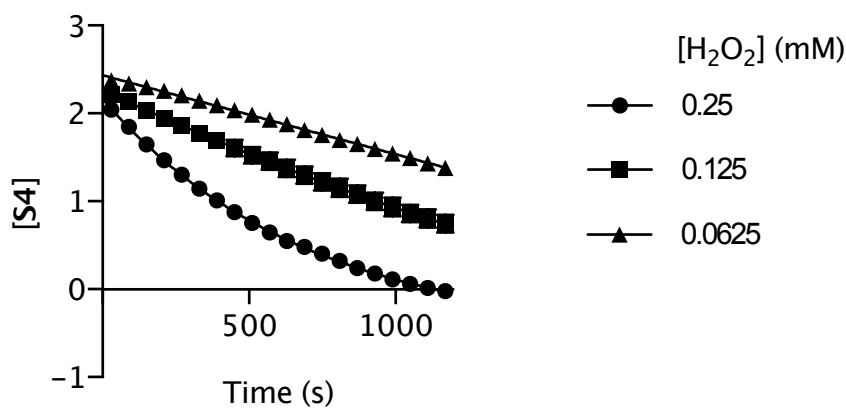


Figure S8. Plot of [S4] vs time.

With the known values of [S4] from Table S5, $\ln[S4]$ vs time (s) was plotted to obtain observed rate constants k' as the slope of the linear plot (Figure S11).

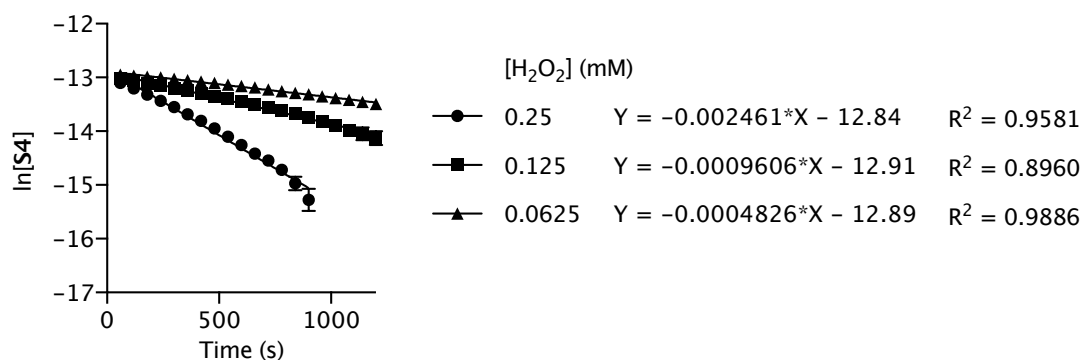


Figure S9. Plot of $\ln[S4]$ vs time.

From the plot of $\ln[S4]$ vs time, pseudo 1st order rate constant was obtained as follows:

[H ₂ O ₂] (mM)	k' (s ⁻¹)
0.25	0.002461
0.125	0.0009606
0.0625	0.0004826

The tabulated values of k' were plotted against [H₂O₂] to obtain 2nd order rate constant.

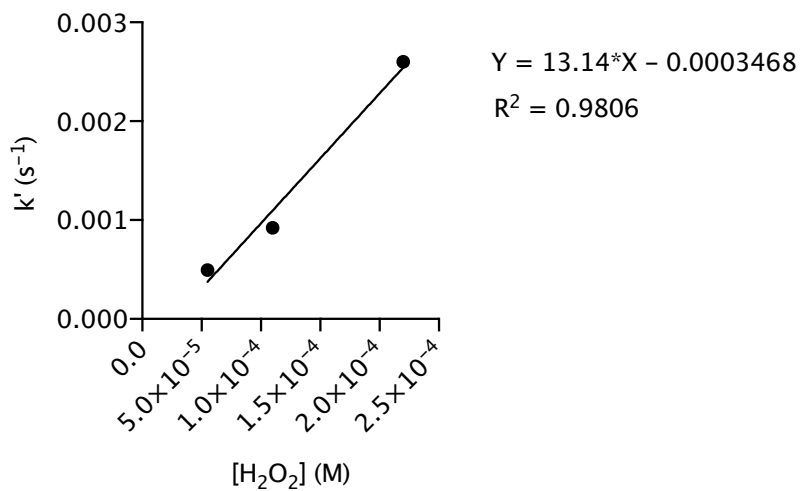


Figure S10. Plot of k' vs [H₂O₂].

The second order rate constant was obtained as $k = 9.33 \pm 0.64 \text{ M}^{-1} \text{ s}^{-1}$

[H ₂ O ₂] (μM)	Fluorescence Intensity		
0	88,783	89,939	87,976
4.47	101,145	105,171	96,139
8.94	116,525	120,542	109,368
17.88	156,244	154,498	141,321
35.75	274,321	249,220	231,325
71.50	555,126	501,632	506,569
143.00	1,069,430	1,068,510	1,025,260

Table S7. Raw fluorescence values for the reaction of **1** with H₂O₂. *n* = 3.

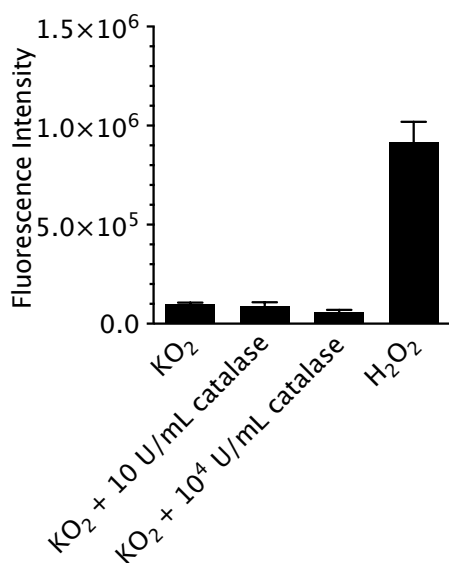


Figure S11. Determining selectivity of **1**: Reaction with O₂^{•-}.

Sample	Fluorescence Intensity		
KO ₂	106,099	92,938	99,300
KO ₂ + 10 U/mL catalase	104,768	72,151	98,514
KO ₂ + 10 ⁴ U/mL catalase	63,553	41,950	67,009
H ₂ O ₂	937,451	1,008,330	803,382

Table S8. Raw fluorescence values for determining selectivity of **1**: Reaction with O₂^{•-}. *n* = 3.

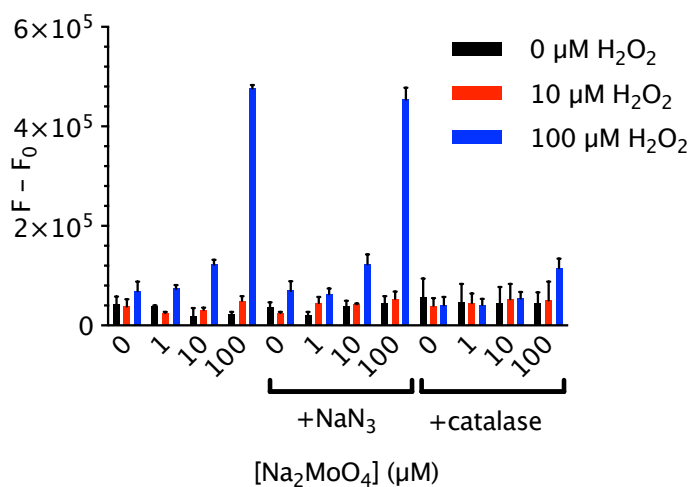


Figure S12. Determining selectivity of **1**: Reaction with $^1\text{O}_2$.

Additive	[Na Mo O ₄] (μM)	0 μM H ₂ O ₂			10 μM H ₂ O ₂			100 μM H ₂ O ₂		
	0	59,711	30,413	38,407	34,413	26,177	54,164	86,970	68,803	48,948
	1	36,829	38,478	40,456	27,103	23,437	25,142	74,322	79,262	64,673
	10	1,067	29,637	27,490	33,243	34,233	26,543	132,450	119,014	113,217
	100	24,734	26,617	17,702	38,768	55,874	53,722	476,166	482,448	468,686
NaN ₃	0	47,427	27,816	33,822	22,037	25,574	26,509	47,879	71,128	86,779
NaN ₃	1	17,056	15,590	28,737	47,687	30,921	55,460	58,618	52,801	75,276
NaN ₃	10	48,985	26,189	39,286	41,011	44,837	41,481	99,199	137,922	128,720
NaN ₃	100	41,150	60,360	31,422	36,764	62,417	61,596	459,433	473,881	427,359
catalase	0	47,781	25,839	97,988	24,872	37,852	55,740	24,774	36,194	57,786
catalase	1	32,277	18,911	88,941	25,228	47,957	62,449	34,302	31,904	54,776
catalase	10	30,189	24,960	82,044	31,421	39,031	88,171	39,161	54,221	66,499
catalase	100	27,512	34,883	69,835	25,678	32,090	94,073	103,725	102,097	137,047

Table S9. Raw fluorescence values for determining selectivity of **1**: Reaction with $^1\text{O}_2$. Data shown are the fluorescence at 40 min minus the fluorescence at 0 min. $n = 3$.

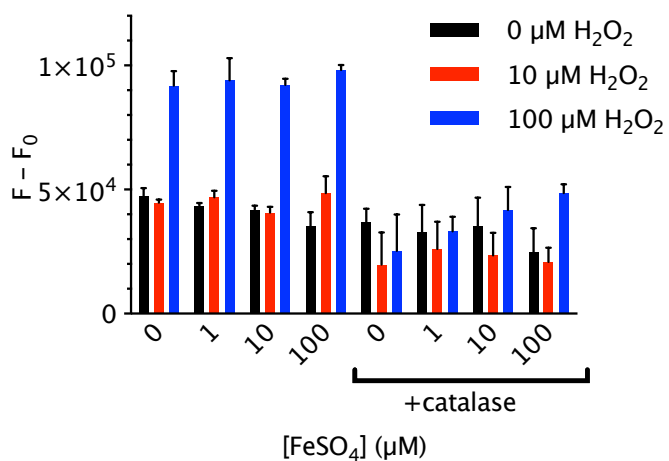


Figure S13. Determining selectivity of 1: Reaction with $\bullet\text{OH}$.

Additive	$[\text{FeSO}_4]$ (μM)	0 μM H_2O_2			10 μM H_2O_2			100 μM H_2O_2		
		0	50,173	48,124	44,143	43,929	46,186	43,989	94,742	95,713
1	44,775	42,847	41,775	49,425	47,262	44,251	103,905	91,684	86,594	
10	43,299	42,365	40,214	42,933	40,908	38,283	90,712	94,948	91,049	
100	32,709	41,651	31,615	56,260	46,281	43,358	99,391	95,778	99,384	
catalase	0	31,506	41,640	38,159	16,840	33,959	8,517	37,819	28,926	9,145
catalase	1	28,688	24,659	45,310	31,319	13,633	33,399	34,591	26,790	38,285
catalase	10	24,822	33,920	47,376	19,991	16,693	33,776	42,724	50,635	32,300
catalase	100	35,828	18,194	20,321	20,486	26,765	15,423	46,921	52,666	46,232

Table S10. Raw fluorescence values for determining selectivity of 1: Reaction with $\bullet\text{OH}$. Data shown are the fluorescence at 40 min minus the fluorescence at 0 min. $n = 3$.

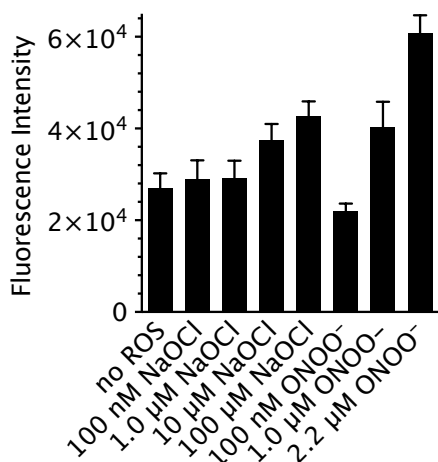


Figure S14. Determining selectivity of **1**: Reaction with ClO⁻ and ONOO⁻.

	Fluorescence Intensity		
no ROS	30,591	24,478	26,025
100 nM NaOCl	33,503	25,413	28,088
1.0 μM NaOCl	28,551	25,590	33,211
10 μM NaOCl	41,611	35,271	35,308
100 μM NaOCl	46,362	40,070	41,695
100 nM ONOO ⁻	23,606	21,961	20,229
1.0 μM ONOO ⁻	46,271	39,358	35,209
2.2 μM ONOO ⁻	63,954	56,351	61,987

Table S11. Raw fluorescence values for determining selectivity of **1**: Reaction with ClO⁻ and ONOO⁻. *n* = 3.

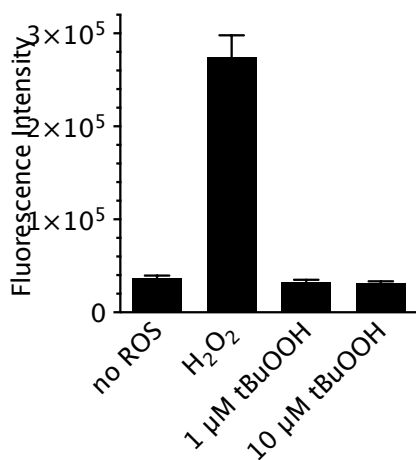


Figure S15. Determining selectivity of **1**: Reaction with ^tBuOOH

	Fluorescence Intensity		
no ROS	34,525	36,401	39,836
H ₂ O ₂	277,013	296,506	250,145
1 μM ^t BuOOH	32,951	29634	34,860
10 μM ^t BuOOH	31,650	28,922	33,363

Table S12. Raw fluorescence values for Determining selectivity of 1: Reaction with ^tBuOOH. *n* = 3.

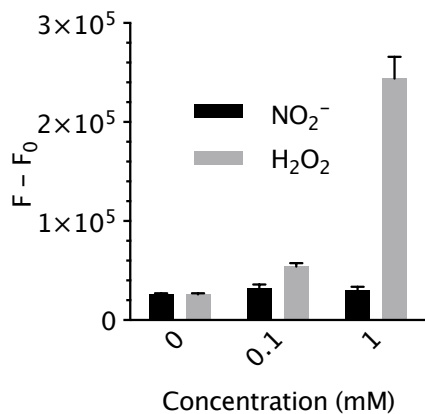


Figure S16. Determining selectivity of 1: Reaction with NO₂⁻. *n* = 3.

[NO ₂ ⁻] or [H ₂ O ₂] (μM)	NO ₂ ⁻			H ₂ O ₂		
0	24,359	26,870	26,226			
0.1	31,075	36,429	27,504	58,172	52,104	52,249
1	26,768	31,470	33,004	266,770	242,313	222,834

Table S13. Raw fluorescence values for determining selectivity of 1: Reaction with NO₂⁻. Data shown are the fluorescence at 15 min minus the fluorescence at 0 min. *n* = 3.

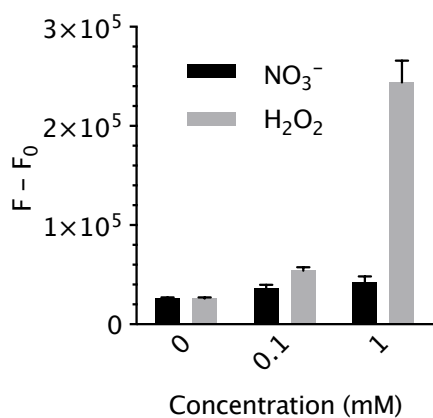


Figure S17. Determining selectivity of **1**: Reaction with NO₃⁻. *n* = 3.

[NO ₃ ⁻] or [H ₂ O ₂] (μM)	NO ₃ ⁻			H ₂ O ₂		
	0	24,359	26,870	26,226		
0.1	34,507	35,439	40,487	58,172	52,104	52,249
1	43,966	35,385	47,433	266,770	242,313	222,834

Table S14. Raw fluorescence values for determining selectivity of **1**: Reaction with NO₃⁻. Data shown are the fluorescence at 15 min minus the fluorescence at 0 min. *n* = 3.

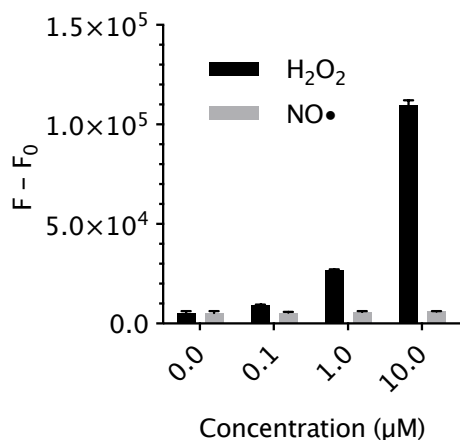


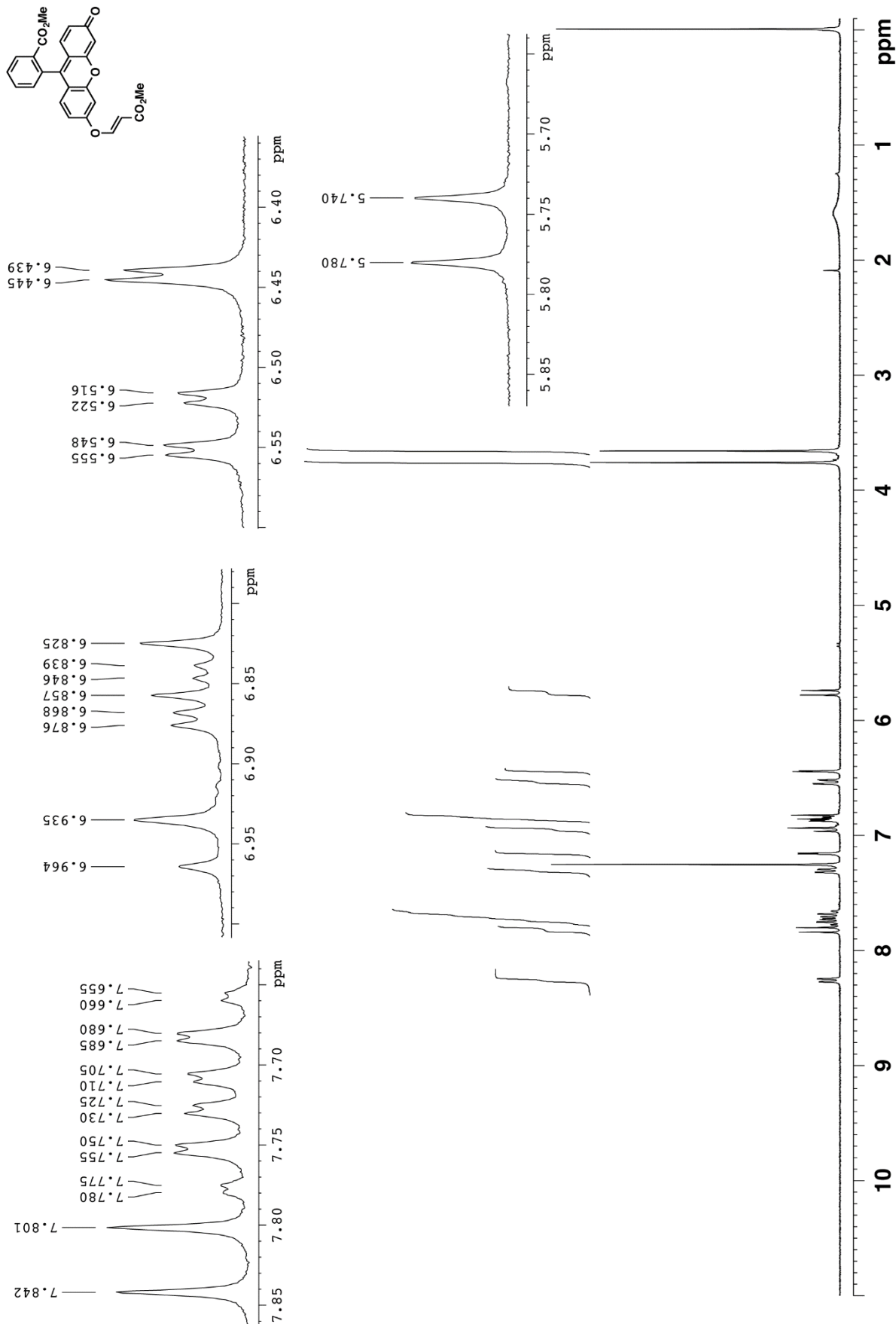
Figure S18. Determining selectivity of **1**: Reaction with NO•. *n* = 3.

[NO•] or [H ₂ O ₂] (μM)	NO•			H ₂ O ₂		
	0	4,567	5,018	6,300		
0.1	5,344	5,827	5,393	9,370	9,525	9,517
1	6,268	5,961	5,430	26,155	26,618	27,176
10	6,104	6,207	5,735	111,008	106,765	111,053

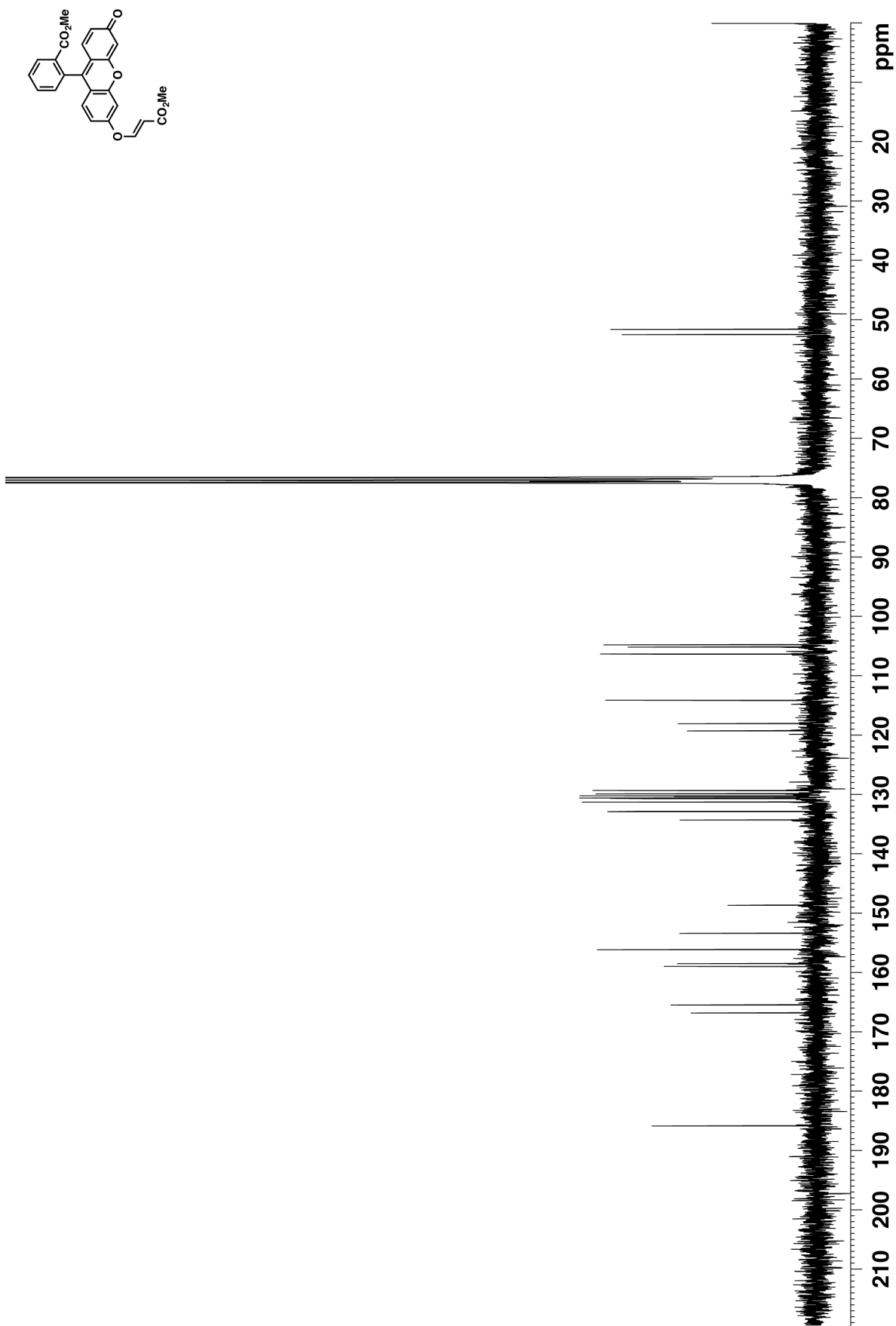
Table S15. Raw fluorescence values for Determining selectivity of **1**: Reaction with NO•. Data shown are the fluorescence at 15 min minus the fluorescence at 0 min. *n* = 3.

References:

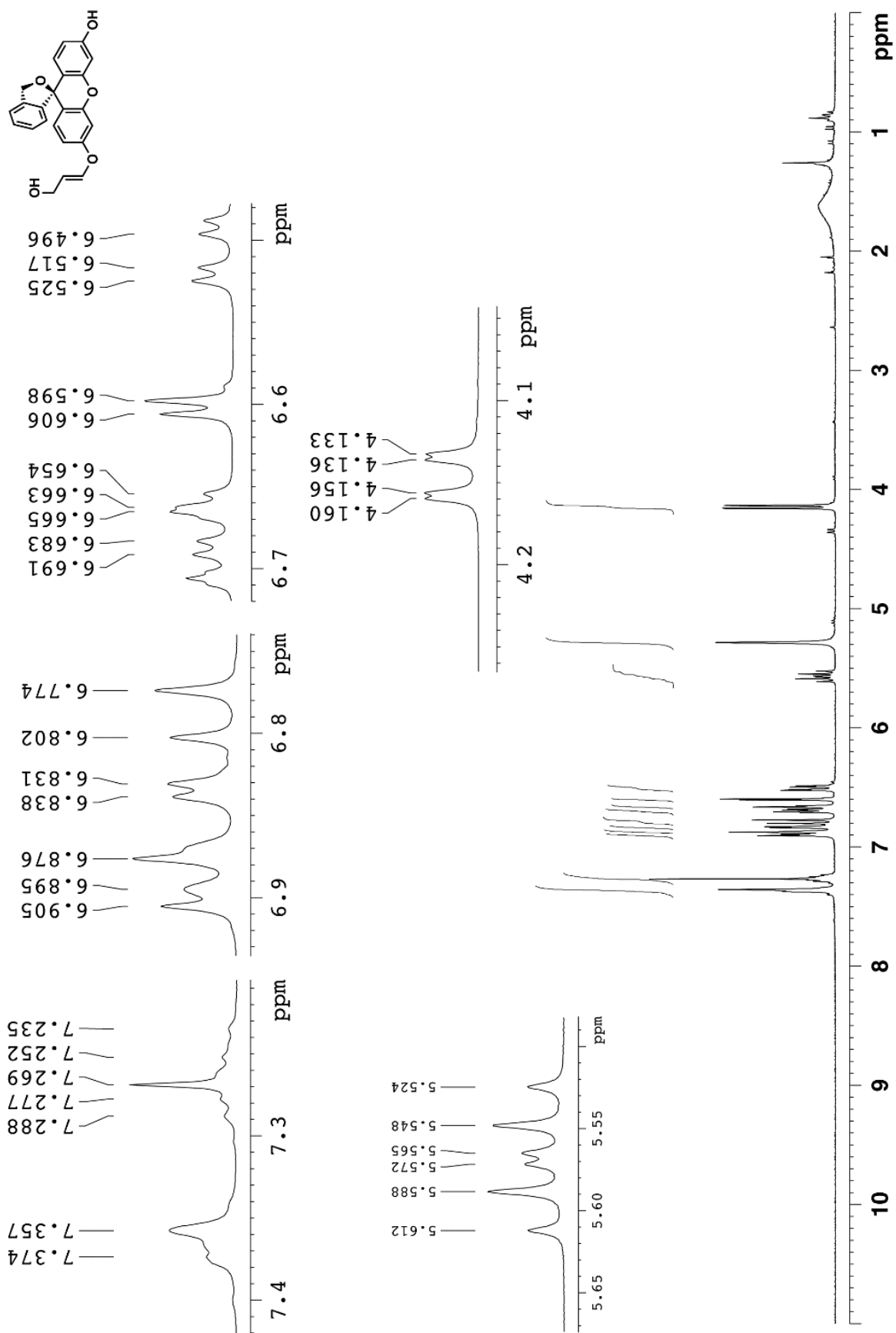
1. L. Ying; B. P. Bruce; *Bioconj. Chem.*, **2011**, *22*, 987–992.
2. S. Ando, K. Koide; *J. Am. Chem. Soc.* **2011**, *133*, 2556–2566.
3. A. Krief, F. Lonz; *Tetrahedron Lett.* **2002**, *35*, 6255–6257.



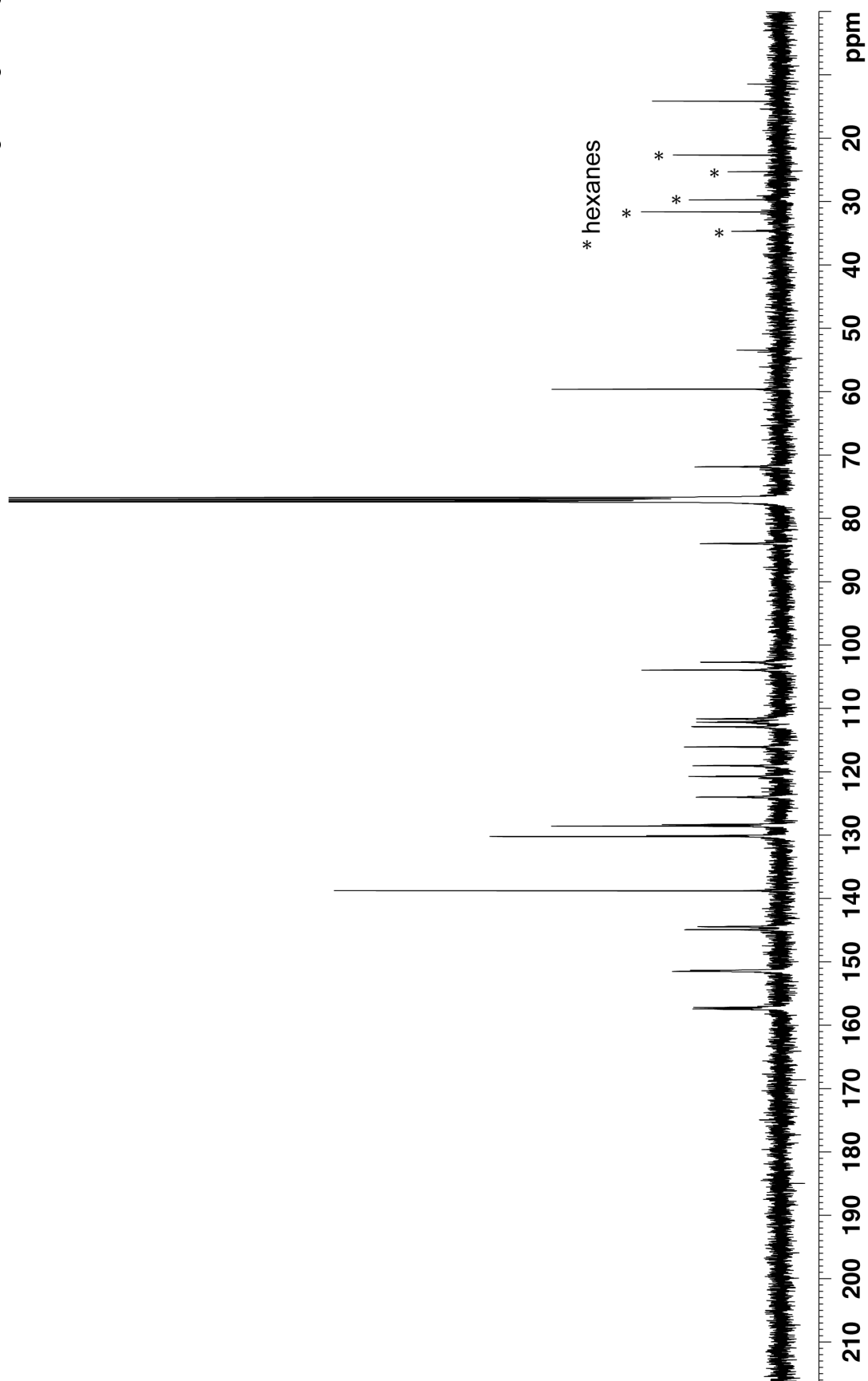
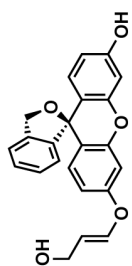
Spectrum 1. ¹H NMR spectrum of **8** (300 MHz, CDCl₃, 293K).



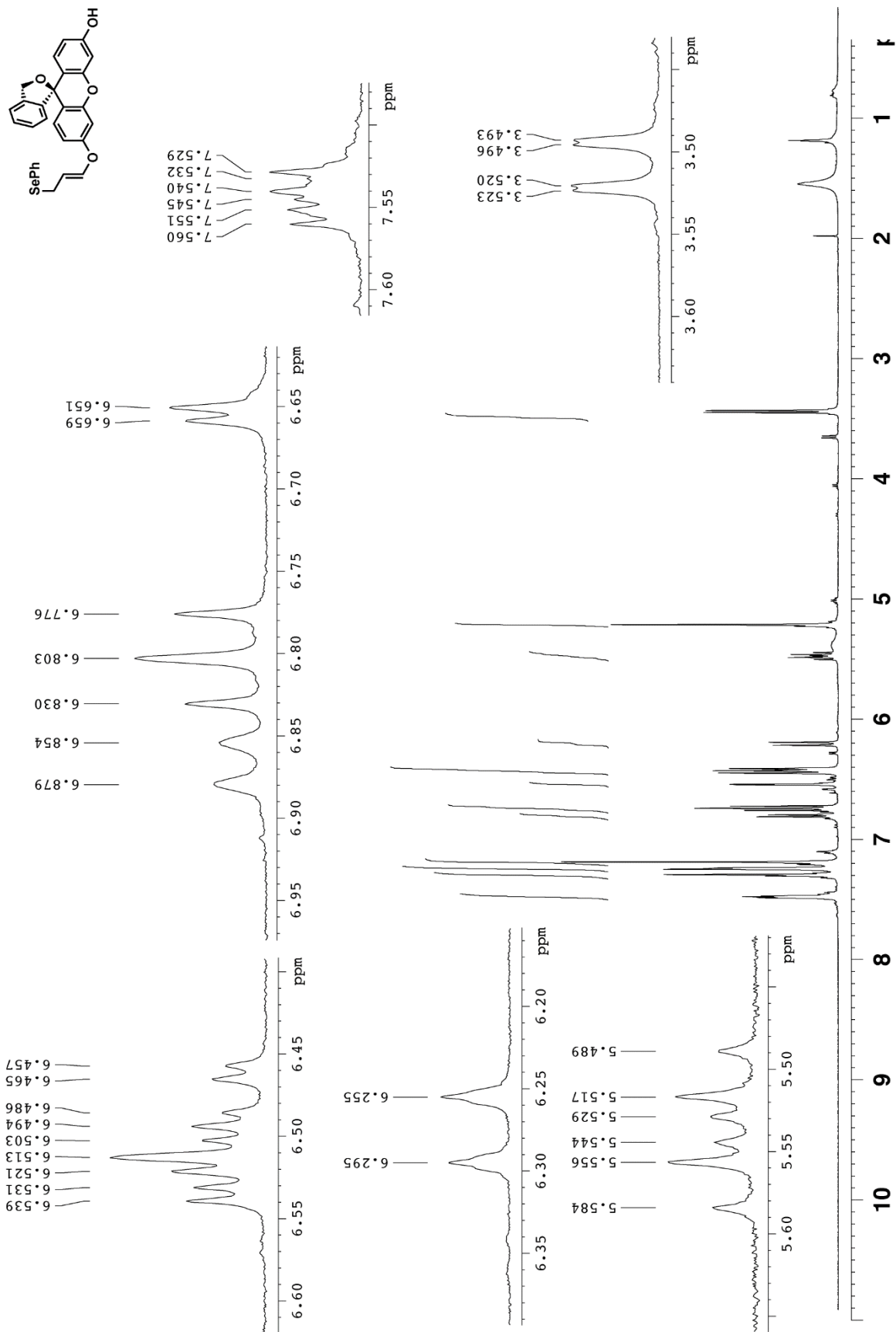
Spectrum 2. ^{13}C NMR spectrum of **8** (75 MHz, CDCl_3 , 293K).



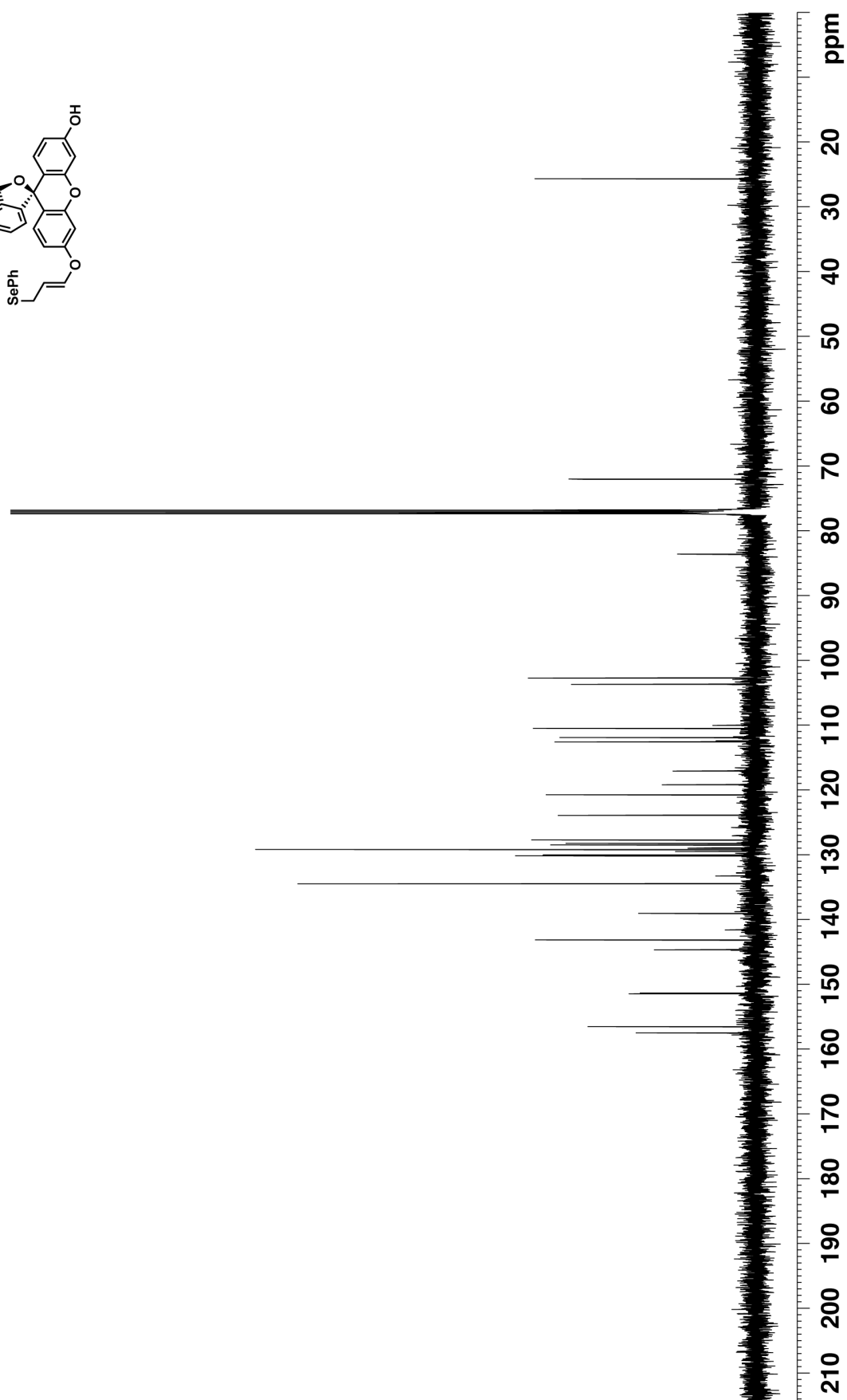
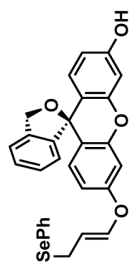
Spectrum 3. ^1H NMR spectrum of **9** (300 MHz, CDCl_3 , 293K).



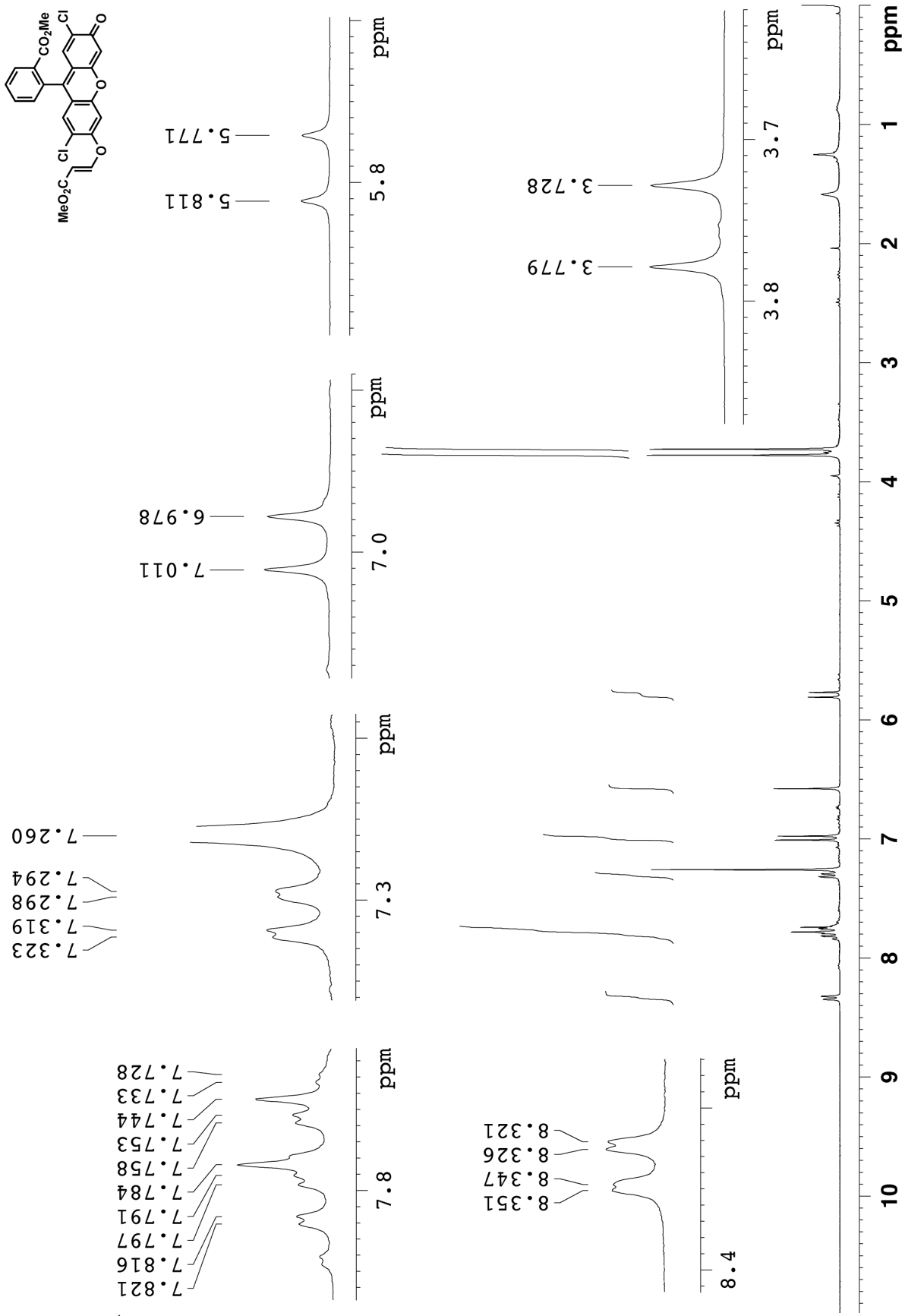
Spectrum 4. ^{13}C NMR spectrum of **9** (100 MHz, CDCl_3 , 293K).



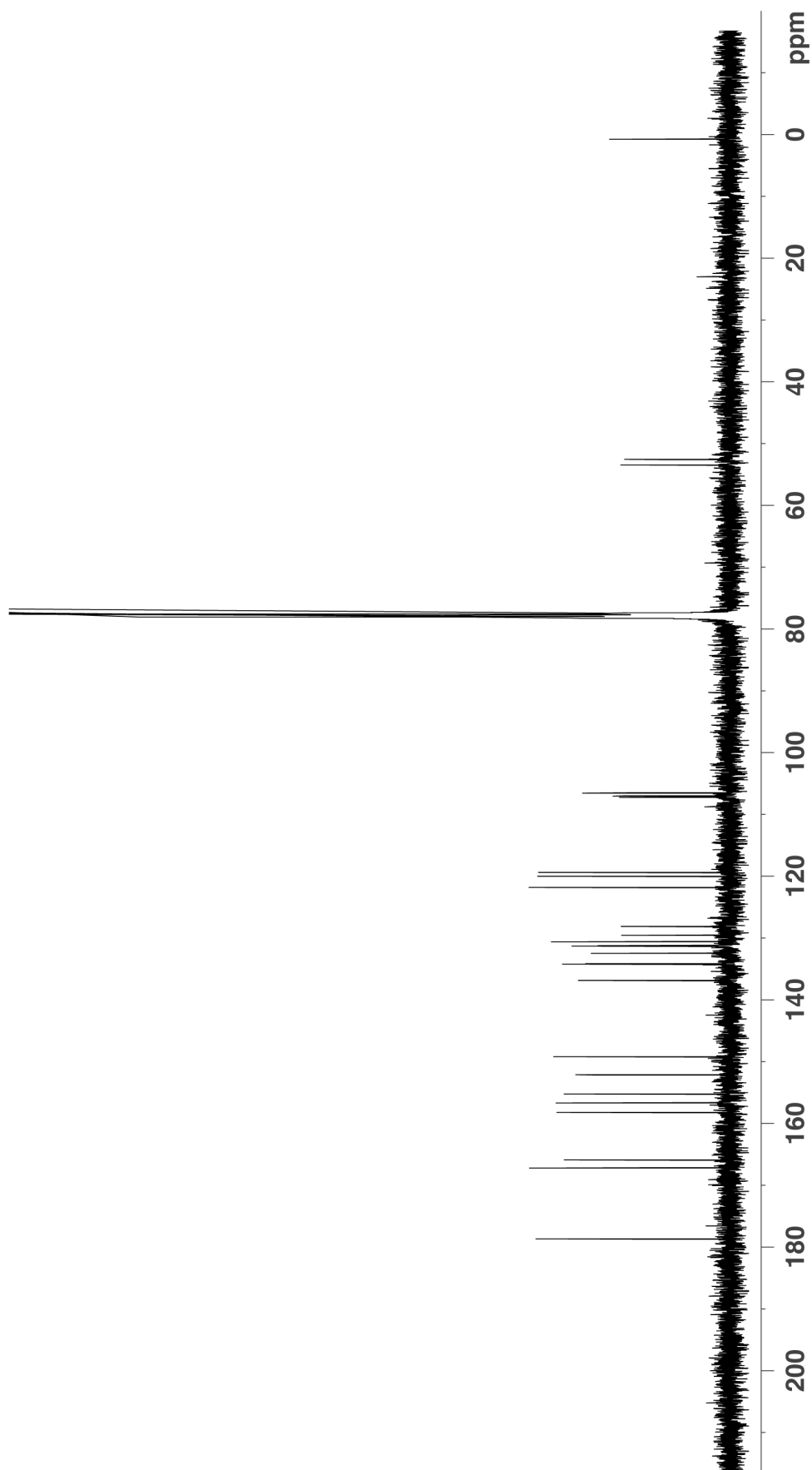
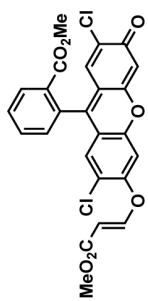
Spectrum 5. ^1H NMR spectrum of **1** (300 MHz, CDCl_3 , 293K).



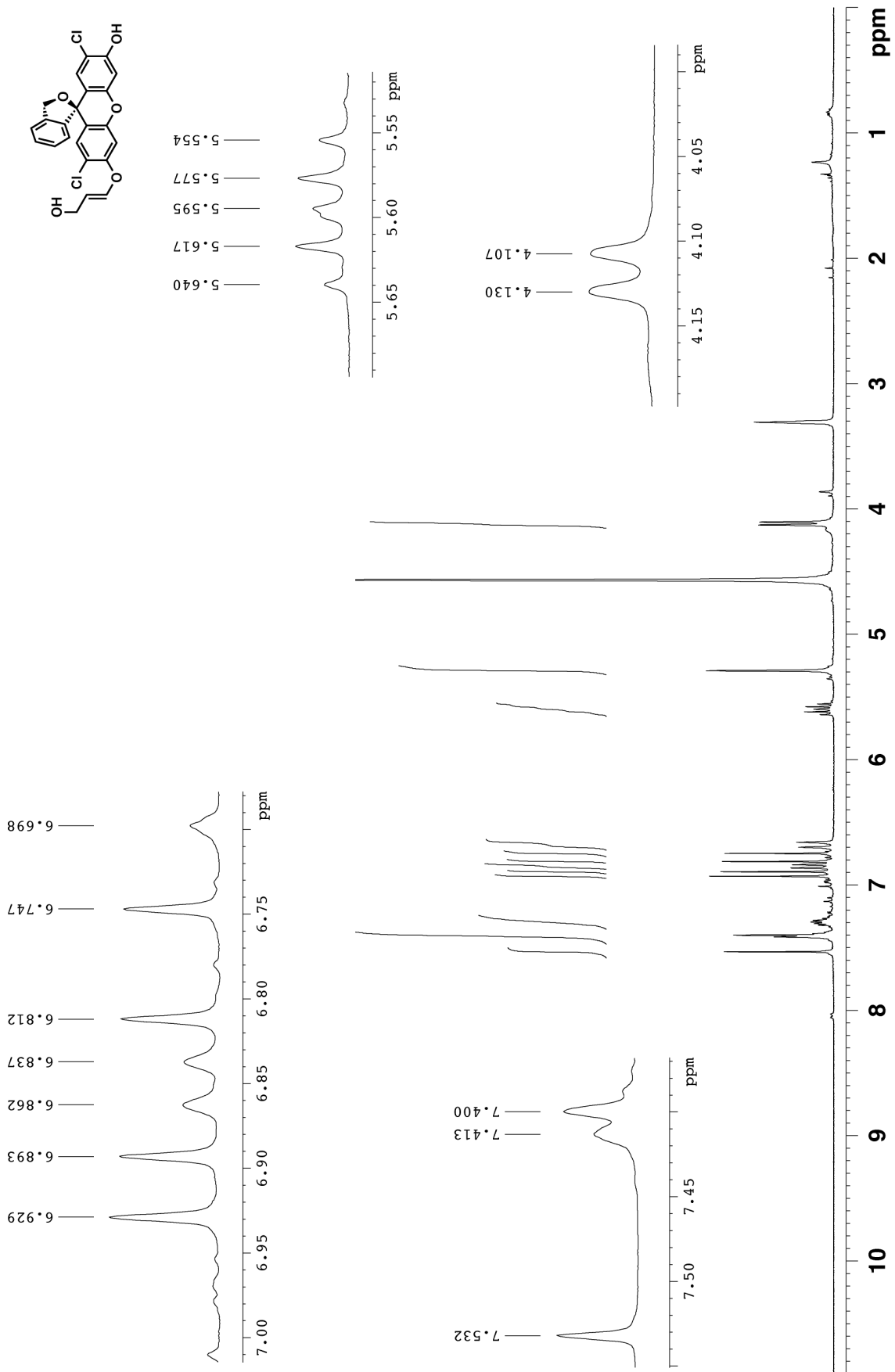
Spectrum 6. ^{13}C NMR spectrum of **1** (125 MHz, CDCl_3 , 293K).



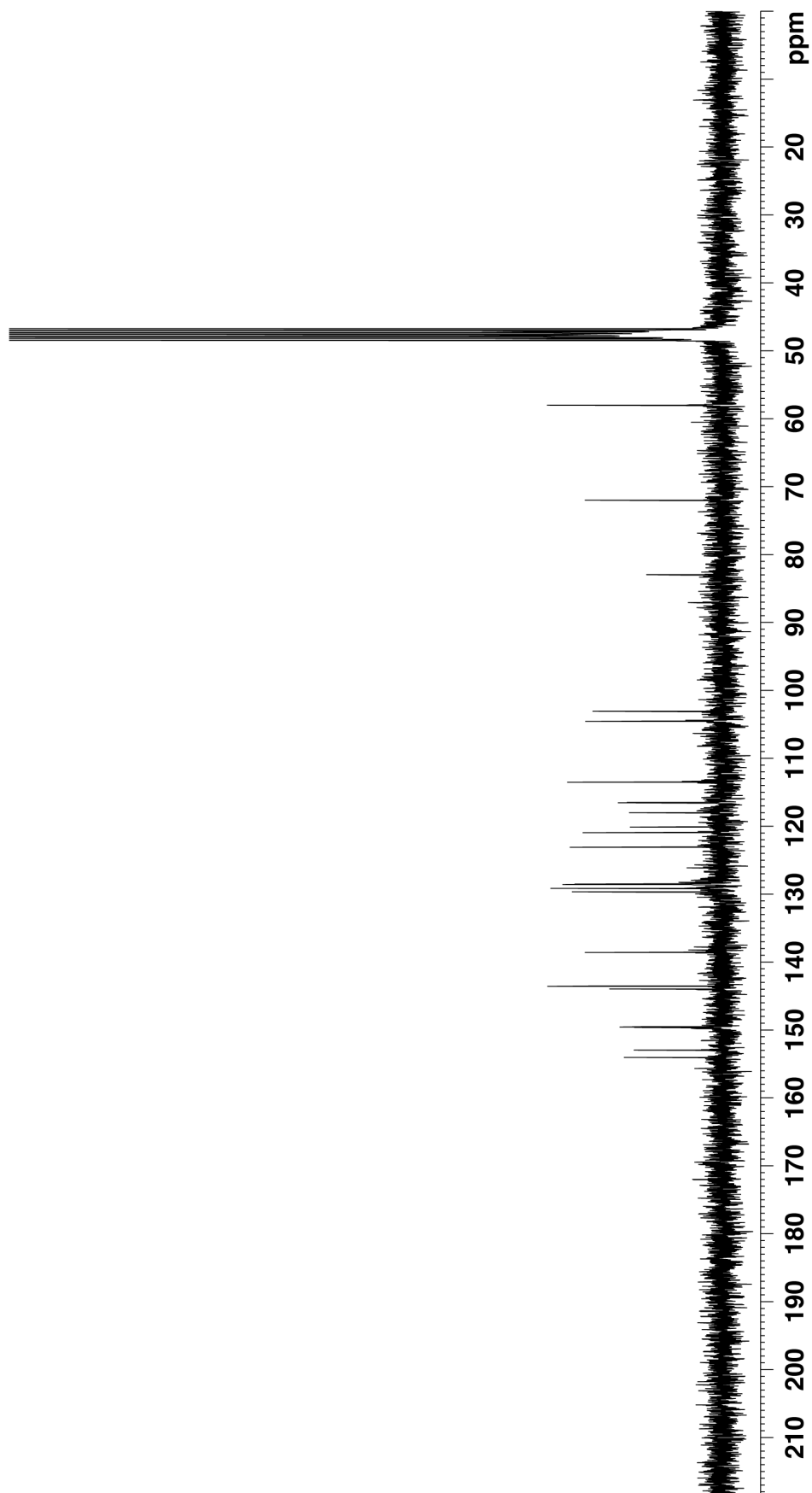
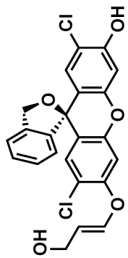
Spectrum 7. ¹H NMR spectrum of **S2** (300 MHz, CDCl₃, 293K).



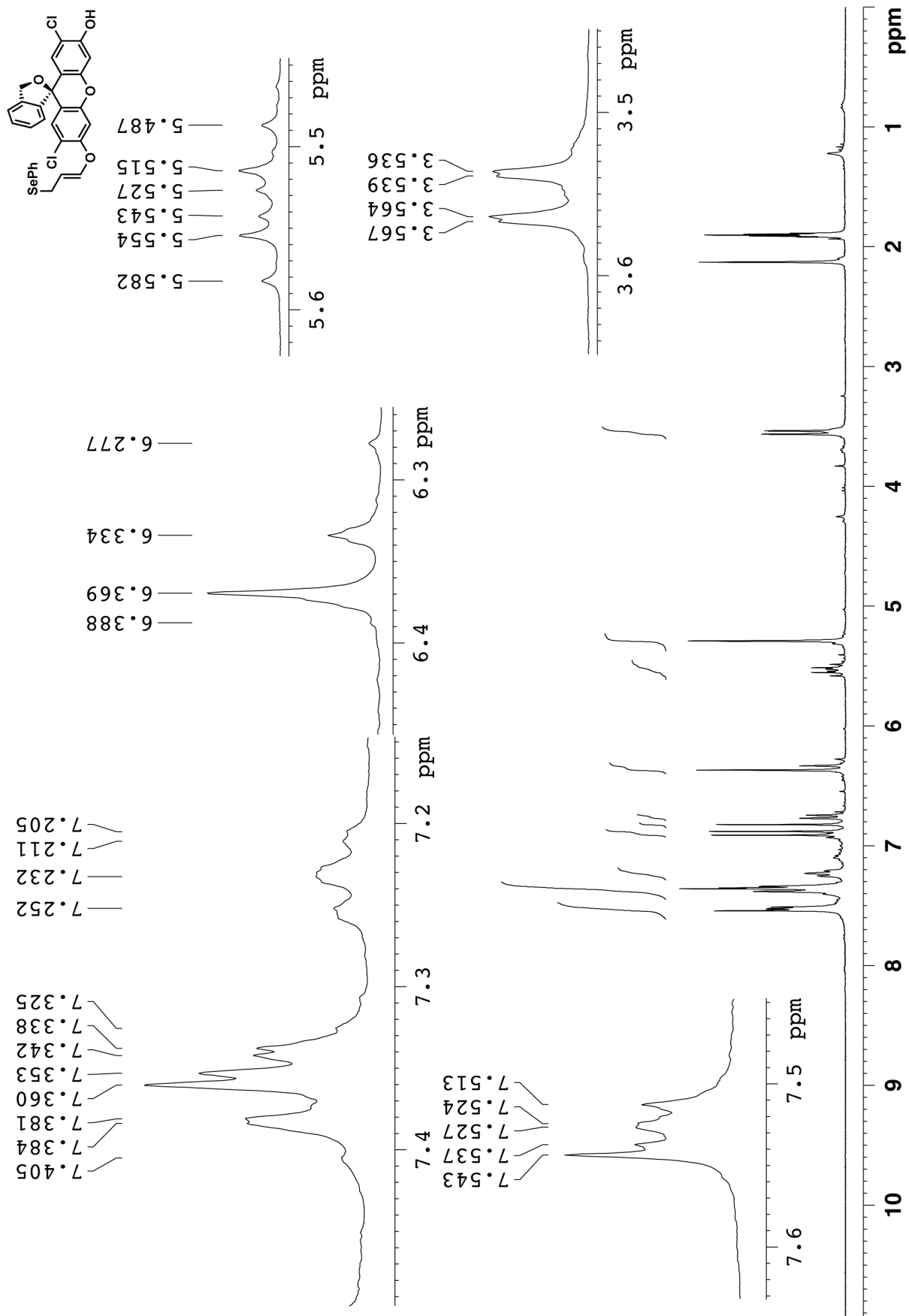
Spectrum 8. ^{13}C NMR spectrum of **S2** (100 MHz, CDCl_3 , 293K).



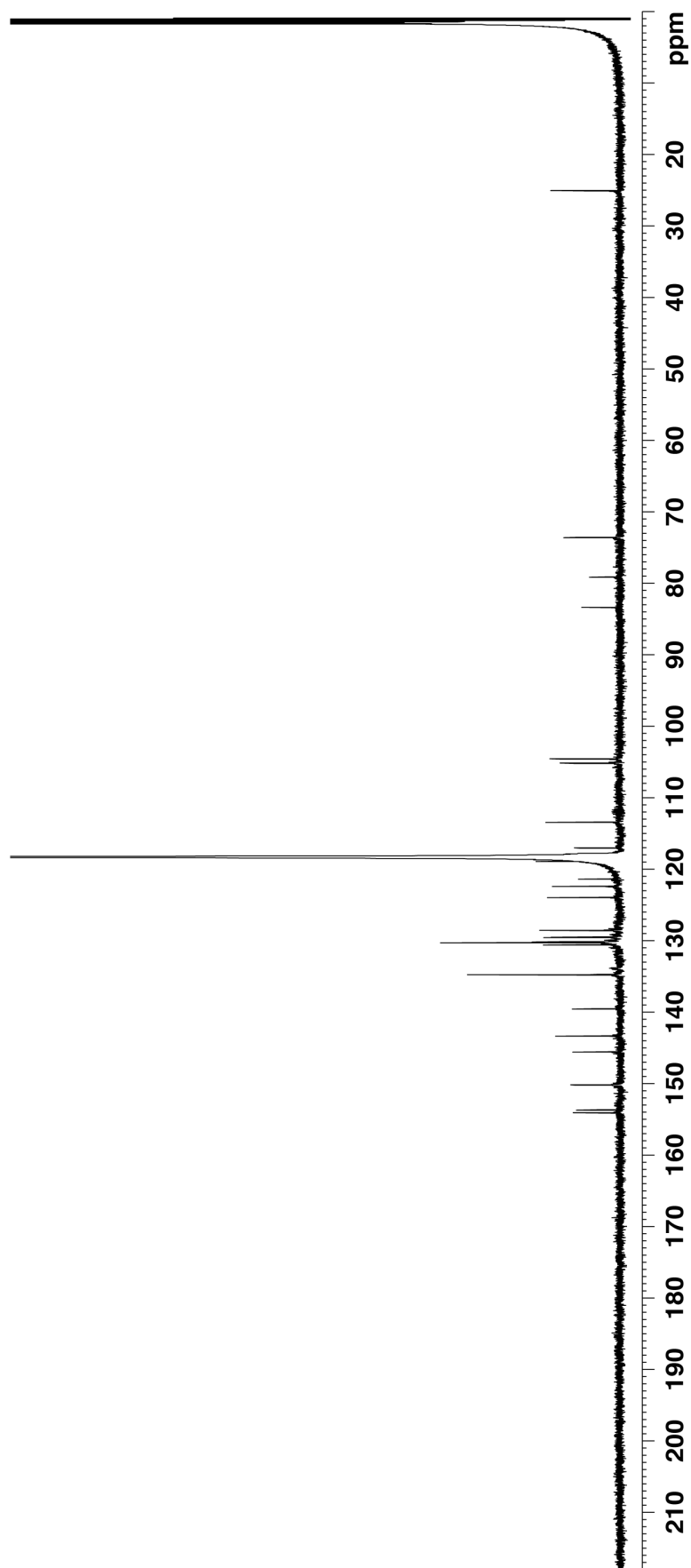
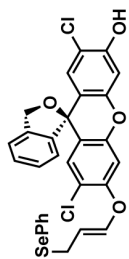
Spectrum 9. ¹H NMR spectrum of **S3** (300 MHz, CD₃OD, 293K).



Spectrum 10. ¹³C NMR spectrum of **S3** (75 MHz, CD₃OD, 293K).



Spectrum 11. ¹H NMR spectrum of **S4** (300 MHz, CD₃CN, 293K).



Spectrum 12. ^{13}C NMR spectrum of **S4** (150 MHz, CD_3CN , 293K).